Mass Transfer on Multiphase Transitions in Low-Temperature Carbon-Dioxide Floods

R. Okuno, SPE, and **Z. Xu,** SPE, University of Alberta

Summary

Mixtures of reservoir oil and carbon dioxide (CO_2) can exhibit complex multiphase behavior at temperatures typically less than 120°F, in which a third CO_2-rich liquid (L_2) phase can coexist with the oleic (L_1) and gaseous (V) phases. The three-phase behavior is bounded by two types of critical endpoints (CEPs) in composition space. The lower CEP (LCEP) is a tie line in which the two liquid phases merge in the presence of the V phase, and the upper CEP (UCEP) is a tie line in which the L_2 and V phases merge in the presence of the L_1 phase. Slimtube tests reported in the literature show that low-temperature oil displacement by CO_2 can result in the high displacement efficiency of more than 90% when three phases are present during the displacement. The nearly piston-like displacements can be quantitatively reproduced in numerical simulations when the CEP behavior is properly considered. However, it is uncertain how multicontact miscibility (MCM) is developed through the interaction of flow and three-hydrocarbon-phase behavior.

This research presents a detailed analysis of mass conservation on multiphase transitions between two and three phases for the limiting three-phase flow, where the L_1 phase is completely displaced by the L_2 phase on the LCEP. The analysis indicates that interphase mass transfer on multiphase transitions occurs in the most-efficient way for MCM development. Simple analytical conditions derived for MCM through three phases are applied to 1D fine-scale simulations of CO_2 floods by use of four and more components. Results show that the MCM conditions are nearly satisfied when the effect of numerical dispersion is small. MCM is likely developed through three hydrocarbon phases on the LCEP in the cases studied. This is consistent with analytical solutions of water and gas injection presented in the literature, in which MCM is developed on a CEP for the aqueous, V, and L_1 phases. For MCM cases in this research, the L_2-V two phases are present upstream of the miscible front if the composition path does not go through the UCEP tie line. However, they also can be miscible on the non-L_1 edge of the UCEP tie line if the MCM composition path goes through it.

Three-phase flow gradually changes to two-phase flow with varying pressure in the presence of numerical dispersion. It is shown that interphase mass transfer on multiphase transitions becomes less efficient during the change until the three-phase region completely disappears.

Introduction

Mixtures of reservoir oil and CO_2 can exhibit complex multiphase behavior at temperatures typically less than 120°F, in which a third CO_2-rich liquid (L_2) phase can coexist with the oleic (L_1) and gaseous (V) phases (e.g., Huang and Tracht 1974; Shelton and Yarborough 1977; Metcalfe and Yarborough 1979; Gardner et al. 1981; Henry and Metcalfe 1983; Orr and Jensen 1984; Turek et al. 1988; Khan et al. 1992; Creek and Sheffield 1993). Because of the complexity, phase behavior and oil-displacement mechanisms were studied for low-temperature CO_2 floods in various ways, such as single- and multiple-contact measurements, slimtube displacements, and numerical simulations with an equation of state (EOS).

Multiphase behavior of CO_2/reservoir-oil mixtures is conventionally presented with a pressure-composition (P-x) diagram (Orr and Jensen 1984; Turek et al. 1988; Creek and Sheffield 1993). Three-phase equilibrium L_1-L_2-V occurs within a reservoir-pressure range at high CO_2 concentrations on a P-x diagram at temperatures typically less than 120°F. Two-liquid phases can coexist at higher pressures above the three-phase region. Creek and Sheffield (1993) found no upper boundary of the L_1-L_2 envelope up to 18,000 psia for the CO_2/reservoir-oil mixtures studied. Turek et al. (1988) observed no critical point for L_1-L_2 for the CO_2/west-Texas-oil mixtures studied. An L_2-V region can exist at pressures above a three-phase region at very high CO_2 concentrations [e.g., more than 99.0% in Turek et al. (1988)]. Creek and Sheffield (1993) reported that the L_2 phase became denser than the L_1 phase at pressures higher than 16,500 psia in the L_1-L_2 region in their experiments.

A P-x diagram represents a cross section of phase behavior along the mixing line between two compositions at a fixed temperature. Thus, a P-x diagram shows only a small portion of phase behavior that spans pressure-temperature-composition (P-T-x) space of $(N_C + 1)$ dimensions, where N_C is the number of components. Turek et al. (1988) observed in their single-contact measurements for west-Texas oils and CO_2 that the L_2 phase had a similar composition to the V phase in the three-phase region. On the basis of this observation, they stated that the three-phase region exists within a narrow pressure range, in which the L_2 phase vaporizes with decreasing pressure. When P-T-x space is properly considered, however, their observation indicates that the mixing ratio of the oil and CO_2 gave a composition near a CEP.

A CEP is a critical state in which two of the three equilibrium phases become critical (Uzunov 1993). There are two types of CEPs for mixtures of CO_2 and hydrocarbons—LCEP in which the L_1 and L_2 phases merge in the presence of the V phase ($L_1 = L_2$-V), and UCEP in which the V and L_2 phases merge in the presence of the L_1 phase (L_1-L_2 = V). That is, what Turek et al. (1988) observed in their measurements is an overall composition near an UCEP.

A three-phase region for oil/CO_2 mixtures can be considered to be bounded by the LCEP and UCEP in composition space. Appendix A presents a schematic for such a bounded three-phase region for four components (Okuno et al. 2011). Four is the minimal number of components required to develop CEP behavior in composition space at a temperature and pressure, as predicted by the phase rule for critical points (Okuno 2009). A CEP is a tie line, instead of a point, as shown in **Fig. A-1.** Therefore, a CEP is sometimes called a CEP tie line to avoid potential confusion in this paper.

Three-phase behavior bounded by the two CEPs was observed for hydrocarbon mixtures (Rowlinson and Freeman 1961; Davenport and Rowlinson 1963; Davenport et al. 1966; Kohn et al. 1966; Wagner et al. 1968) and CO_2/n-C_{13} mixtures (Enick et al. 1985; Galindo and Blas 2002). Modeling of the complex three-phase behavior was also conducted with various EOSs [e.g., the van der Waals EOS (van Konynenburg 1968; Scott and van Konynenburg 1970; van Konynenburg and Scott 1980; Bluma and Dieters 1999), the Redlich-Kwong EOS (Deiters and Schneider 1976; Deiters and Pegg 1989), the Peng-Robinson (PR) EOS (Gauter 1999; Gauter et al. 1999; Mushrif 2004; Yang 2006; Mushrif and Phoenix 2008), and the Soave-Redlich-Kwong

This paper (SPE 166345) was accepted for presentation at the SPE Annual Technical Conference and Exhibition, New Orleans, Louisiana, USA, 30 September–2 October 2013, and revised for publication. Original manuscript received for review 28 June 2013. Revised manuscript received for review 30 January 2014. Paper peer approved 5 February 2014.

(SRK) EOS (Gregorowicz and de Loos 1996)]. Their results show that a cubic EOS is capable of predicting three-phase behavior (van Konynenburg 1968).

The characterization of reservoir fluids with a cubic EOS was not fully developed for reliable predictions of three-phase behavior. Nevertheless, the static phase behavior of reservoir-oil/CO_2 mixtures was reasonably correlated with the PR EOS (Larson et al. 1989; Khan et al. 1992; Creek and Sheffield 1993) and the SRK EOS (Coutinho et al. 1995). Khan et al. (1992) quantitatively matched slimtube test data for west-Texas oils and CO_2 with the UTCOMP simulator with the PR EOS. The UTCOMP is an EOS compositional multiphase reservoir simulator capable of handling three hydrocarbon phases (Chang et al. 1990).

There are several characteristics of low-temperature oil displacements by CO_2 that are not observed in oil displacements involving only *L-V* two phases. CO_2 breakthrough in these displacements can occur at more than 1.0 pore-volume injected (PVI) and, in many cases, well after 1.2 PVI (Orr et al. 1983; Khan 1992; Creek and Sheffield 1993; Grigg and Siagian 1998). Orr et al. (1983) stated that this late breakthrough is because CO_2 significantly increases its density on dissolution in the L_1 phase. Creek and Sheffield (1993) stated that this late breakthrough is a result of the large molar volume difference between the V and L_2 phases, and called it the volume-charging effect.

Slimtube tests reported in the literature show that low-temperature oil displacement by CO_2 can result in high displacement efficiency of more than 90% when three phases are present during the displacement (Yellig and Metcalfe 1980; Gardner et al. 1981; Orr et al. 1981, 1983; Henry and Metcalfe 1983; Khan 1992; Creek and Sheffield 1993). Appendix B shows schematics of phase behavior present in two- and three-hydrocarbon-phase displacements in one dimension. Minimum miscibility pressures (MMPs) measured in CO_2 slimtube tests were based on a variety of criteria (Holm and Josendal 1980; Yellig and Metcalfe 1980; Negahban and Kremesec 1992; Creek and Sheffield 1993).

Orr et al. (1981) pointed out that measured CO_2-MMPs do not necessarily mean the thermodynamic MMP, although they are likely sufficient to ensure high displacement efficiency. The thermodynamic MMP is a minimum displacement pressure at which complete miscibility between two phases is developed along the composition path from the injection to the initial composition for a 1D isothermal oil displacement in the absence of dispersion (Johns 1992). Several different correlations were proposed on the basis of measured MMPs for CO_2 floods. However, they can be in large error (Stalkup 1978; Holm and Josendal 1980) because oil-displacement mechanisms cannot be reflected properly in such correlations.

Okuno et al. (2011) presented a detailed study of three-phase behavior predictions and displacement efficiency for low-temperature CO_2 floods with the UTCOMP simulator. They used four components to conduct a systematic investigation of oil-displacement mechanisms involving three phases bounded by the UCEP and LCEP tie lines. Results showed that the high efficiency of low-temperature oil displacements by CO_2 occurs when the composition path traverses near the UCEP and LCEP tie lines. Oil components are efficiently extracted by the L_2 phase because of near-LCEP behavior at the leading edge of three phases. Near-UCEP behavior at the trailing edge of three phases then allows the L_2 phase to efficiently merge into the V phase. Thus, the L_2 phase serves as a buffer between the immiscible V and L_1 phases within the three-phase region. They also confirmed this displacement mechanism for multicomponent systems on the basis of west-Texas oils.

Although nearly piston-like displacements were simulated with three phases bounded by the CEP tie lines, it was uncertain how MCM can be developed through the CEP behavior. They used the distance between the L_1 and L_2 phase compositions $d_{L1\text{-}L2} = \| \underline{x}_{L1} - \underline{x}_{L2} \|_2$ as a proximity measure for the LCEP tie line, where $\underline{x}_j$ is the composition vector of equilibrium phase j. Similarly, $d_{L2-V} = \| \underline{x}_{L2} - \underline{x}_V \|_2$ was used as a proximity measure for the UCEP tie line. Although $d_{L2\text{-}V}$ monotonically decreased as oil recovery at 2.0 hydrocarbon-pore-volumes injected (HCPVI) became higher, $d_{L1\text{-}L2}$ did not exhibit the same trend. Even though 500 gridblocks were used in most of their 1D simulations with an implicit-pressure explicit-concentration simulator, numerical dispersion effects were significant near the leading edge of three phases because the CO_2 concentration increased from the initial value of 3.37% to more than 90% there (e.g., Figs. 6 and 7 of Okuno et al. 2011). This likely explains the nonmonotonic trend of $d_{L1\text{-}L2}$ with respect to displacement efficiency in their research.

The development of miscibility in gas floods is best analyzed by the method of characteristics (MOC) applied to 1D isothermal compositional flow in porous media in the absence of dispersion (e.g., Orr 2007; Johns 1992; Dindoruk 1992; LaForce 2005). Theory has been well established for gas floods involving simple two-phase equilibrium (Orr 2007). An MCM composition path goes through a two-phase critical point, and is interpreted as the limit of two-phase displacements.

This thermodynamic condition for MCM is commonly used in efficient MMP calculation algorithms (e.g., Johns and Orr 1996; Wang and Orr 1997; Jessen et al. 1998; Ahmadi 2011; Ahmadi and Johns 2011). In general, there are two main steps in these algorithms—The first step is to locate key tie lines, and the second step is to find the minimal pressure at which any one of the key tie lines becomes zero length. This procedure follows the theoretical fact that MCM is developed at the limit of a two-phase flow.

However, the mechanism for MCM development is unknown for a three-hydrocarbon-phase displacement. A method for finding key tie lines and tie triangles also would be important. Because many oil/solvent mixtures exhibit more than two hydrocarbon phases at operating conditions, the understanding of MCM development through three phases is of practical importance for the petroleum industry.

Recent research on analytical solutions for three-phase displacements has significantly improved our understanding of miscibility development in three-phase flow (LaForce and Johns 2005; LaForce et al. 2008a,b; LaForce and Orr 2008, 2009; LaForce 2012). They studied analytical composition paths and miscibility development in water and gas injection with three and four components. The four components used consisted of water, CO_2, and two hydrocarbon components. The quaternary cases with miscible-gas/water injection presented a CEP in composition space, at which the two hydrocarbon phases were critical in the presence of the aqueous (W) phase (i.e., a CEP of type $L_1 = V\text{-}W$). This is the only CEP in composition space in their research because the W phase is immiscible with the hydrocarbon phases. Their results indicated that MCM can be developed not only at the two-phase critical point ($L_1 = V$), but also on the CEP tie line ($L_1 = V\text{-}W$). In such a case, the initial oil in the *L-W* region was completely displaced by CO_2 in the *V-W* region through the CEP tie line.

Okuno and Xu (2014) recently investigated mass conservation on multiphase transitions between two and three phases in three-hydrocarbon-phase displacements **(Fig. B-1).** Simple conditions were derived for multiphase transitions that yield efficient oil displacement by three hydrocarbon phases. Unlike the phase-composition distances such as $d_{L1\text{-}L2}$ and $d_{L2\text{-}V}$ mentioned above, the efficiency conditions in Okuno and Xu (2014) explicitly consider interphase mass-transfer mechanisms for efficient oil recovery with three hydrocarbon phases. These conditions were successfully used to explain a nonmonotonic trend of oil recovery with respect to gas enrichment, which can occur in heavy-oil displacement by solvent (e.g., DeRuiter et al. 1994; Mohanty et al. 1995). Results in their research indicate that mass transfer on multiphase transitions controls oil displacement by three hydrocarbon phases. However, near-miscible displacements were not investigated in detail.

The term "mass transfer" in this paper is used to indicate the interphase mass transfer caused by components' redistribution among equilibrium phases on phase transitions during oil-displacement processes. It is not the mass transfer that occurs within individual phases caused by molecular diffusion.

TABLE 1—EOS PARAMETERS FOR THE SCHRADER BLUFF OIL (GULER ET AL. 2001)

Components	Oil (Mole %)	Gas (Mole %)	Molecular Weight	*Tc* (°R)	*Pc* (psia)	*Vc* (ft^3/lb-mol)	Acentric Factor
CO_2	0.05	81.5	44.01	547.6	1,071.6	0.416	0.2250
C_1	27.22	0.01	16.04	343.0	667.8	1.602	0.0130
C_2	0.41	0.01	30.07	549.8	707.8	2.451	0.0986
C_3	1.05	0.43	44.10	665.7	616.3	3.300	0.1524
C_4	2.12	7.98	58.12	765.3	550.7	4.088	0.2010
C_5	2.00	5.22	72.15	845.4	488.6	4.946	0.2539
C_6	2.26	2.66	84.00	923.0	483.8	5.294	0.2583
$C_{7–9}$	9.87	2.19	145.16	1040.3	415.4	8.553	0.3165
$C_{10–13}$	10.05	0.00	223.26	1199.6	255.4	13.110	0.4255
$C_{14–19}$	14.51	0.00	353.51	1346.6	203.9	23.070	0.5768
$C_{20–35}$	16.42	0.00	554.55	1532.7	158.0	33.253	0.7659
C_{36+}	14.04	0.00	1052.00	1967.3	94.8	83.571	1.1313

In this research, mass transfer on multiphase transitions in low-temperature CO_2 floods is studied. We first investigate possible MCM development through three hydrocarbon phases on the basis of recent analytical results of LaForce et al. (2008a,b; LaForce and Orr 2008, 2009; LaForce 2012). Four components are used so that CEP tie lines can exist in composition space. Mass conservation on multiphase transition is then analyzed when MCM is developed at the limit of three-hydrocarbon phase displacements, in which the main novelty of this research lies. This analysis yields simple analytical conditions for MCM development through three hydrocarbon phases, which can be used in the presence of numerical dispersion. It is also explained how three-phase flow changes to two-phase flow on the basis of mass transfer on multiphase transitions. Finally, simulation case studies are conducted for CO_2 injection for the Bob Slaughter Block oil and the Schrader Bluff (SB) oil. These case studies show the validity of research results in multicomponent oil displacements.

Near Miscibility in Low-Temperature CO_2 Flooding Simulation

In this section, we discuss the development of MCM through three phases. First, analytical research results of LaForce et al. (LaForce et al. 2008a,b; LaForce and Orr 2008, 2009; LaForce 2012) are summarized and interpreted in terms of MCM development. Numerical simulations are then conducted for quaternary oil displacements by CO_2, which exhibit nearly piston-like oil displacement with three hydrocarbon phases. The quaternary oil used is based on an Alaskan heavy oil **(Tables 1 and 2),** and referred to as the HQ (or quaternary heavy) oil. Rigorous confirmation of MCM development, however, requires the analytical solution of a three-hydrocarbon-phase flow with the MOC, which was not presented in the literature and is not the objective of this research.

LaForce et al. (LaForce and Orr 2008, 2009; LaForce 2012) studied miscibility development in 1D water and gas injection with the MOC. Three phases, L_1, V, and W, were characterized with four components consisting of the water, CO_2, and two hydrocarbon components. The PR EOS was used for the L_1 and V phases, and Henry's law was used to model the solubilities of CO_2 and hydrocarbon components in the W phase. The water component did not partition into either hydrocarbon phase, which is a reasonable assumption at low reservoir temperatures.

An L_1-V two-phase envelope showed the critical point ($L_1 = V$) on the water-free ternary subsystem (i.e., CO_2-CH_4-C_{10} and CO_2-C_3-C_{16} for their condensing and vaporizing drive systems, respectively). This critical phase formed a CEP tie line with the W phase: $L_1 = V$-W. The equilibrium W phase was very close to the CO_2-water edge of the quaternary system because the solubilities of hydrocarbon components in the W phase were extremely small. Thus, a large three-phase region was present in quaternary composition space, consisting of the L_1 and V phases on the water-free ternary subsystem and the W phase very close to the CO_2-water edge.

Water/CO_2 mixtures were the injection compositions used. Most of the cases used single-phase oils consisting of the two hydrocarbon components, but L_1-W two-phase mixtures were also considered as initial compositions for a few tertiary gasflooding cases. Thus, the injection compositions were always V-W two phases, and the initial compositions were either single- or two-phase mixtures on the other side of the large three-phase region in composition space.

For single-phase initial compositions, MCM was developed at the $L_1 = V$ critical point (i.e., the hydrocarbon edge of the CEP tie

TABLE 2—BINARY INTERACTION PARAMETERS FOR THE SCHRADER BLUFF OIL (GULER ET AL. 2001)

Components	CO_2	C_1	C_2	C_3	C_4	C_5	C_6	$C_{7–9}$	$C_{10–13}$	$C_{14–19}$	$C_{20–35}$	C_{36+}
CO_2	0.0000											
C_1	0.0716	0.0000										
C_2	0.0940	0.0052	0.0000									
C_3	0.0976	0.0168	0.0039	0.0000								
C_4	0.0940	0.0367	0.0123	0.0000	0.0000							
C_5	0.0903	0.0442	0.0232	0.0000	0.0000	0.0000						
C_6	0.0745	0.0000	0.0307	0.0106	0.0003	0.0000	0.0000					
$C_{7–9}$	0.0919	0.0000	0.0503	0.0221	0.0008	0.0004	0.0000	0.0000				
$C_{10–13}$	0.0986	0.0000	0.0050	0.0026	0.0021	0.0012	0.0000	0.0000	0.0000			
$C_{14–19}$	0.1164	0.1694	0.0451	0.0295	0.0101	0.0100	0.0000	0.0000	0.0000	0.0000		
$C_{20–35}$	0.1164	0.1784	0.0655	0.0557	0.0209	0.0192	0.0000	0.0000	0.0000	0.0000	0.0000	
C_{36+}	0.1635	0.1822	0.1336	0.1246	0.0538	0.0495	0.0000	0.0000	0.0000	0.0000	0.0000	0.0000

TABLE 3—EOS PARAMETERS FOR THE HQ OIL

	Oil (Mole %)	Gas (Mole %)	Molecular Weight	*Tc* (°R)	*Pc* (psia)	Acentric Factor	*Vc* (ft^3/lb-mol)
PC1	28.00	20	16.040	343.08	667.18	0.0080	1.5900
PC2	6.60	80	43.470	628.41	704.10	0.1583	2.9570
PC3	55.30	0	211.60	1496.2	351.54	0.4810	9.0100
PC4	10.10	0	800.30	1747.4	121.01	1.1313	86.940

line) if the water concentration in the injectant was less than a critical value. Otherwise, a water bank was formed at the displacement front that prevented CO_2 from contacting oil effectively, which resulted in the L_1-V-W three-phase flow. The MCM cases exhibited no three-phase flow because the V-W two-phase flow occurred upstream of the miscible front.

For the tertiary flooding cases, MCM was developed on the CEP tie line, at which the phase transition occurred between the L_1-W two phases and the V-W two phases. Thus, the two-phase flow consisted of the L_1-W flow downstream and the V-W flow upstream of the miscible front.

An important point from their research results is that MCM can be developed through three-phase flow as long as the L_1 phase is displaced by a non-L_1 phase that can be critical after multiple contacts. For example, the W phase, which is always immiscible with the L_1 phase, was coinjected with the V phase in the water and gas injection. However, the development of miscibility on a CEP was still possible after multiple contacts of the V phase with the L_1 phase. Then, the phase transition between L_1-W and V-W occurred on the CEP tie line, at which the non-W phase switched its identity from L_1 to V. No three-phase equilibrium happened along the MCM composition path in the absence of dispersion.

The MCM composition paths through a CEP tie line in LaForce and Orr (2008) presented direct shocks from the initial compositions onto the CEP tie line in the vaporizing-drive cases. This indicates that the initial composition must be on or outside of the critical tie-triangle extension plane for a vaporizing drive to develop MCM. The critical tie-triangle extension plane is a plane in composition space that is defined by three equilibrium phases, two of which are critical in the presence of the other immiscible phase. This reduces to the traditional condition for a ternary vaporizing drive with two phases that the initial composition must be on or outside of the critical tie-line extension for miscible flow (Johns 1992). The above-mentioned condition extended for three phases is necessary, but may not be sufficient for MCM development through three phases. The effect of a high-mobility W phase at the initial condition is unknown on such MCM development (LaForce and Orr 2008).

Three-phase behavior in low-temperature CO_2 floods is more involved. The L_2 phase can be miscible with the L_1 phase at the LCEP tie line and with the V phase at the UCEP tie line, as shown in Appendix A. That is, it must be the L_2 phase that develops MCM with the L_1 phase in a three-hydrocarbon-phase flow considered in this research. A comparison with the results of LaForce et al. indicates that the two-phase transition between L_1-V and L_2-V should occur on the LCEP along an MCM composition path as long as the V phase does not prevent the L_2 phase from developing miscibility with the L_1 phase. Unlike the W phase in the water/gas coinjection in LaForce et al., however, the V phase also can be beneficial for the three-hydrocarbon-phase flow to develop miscibility. For example, Okuno et al. (2011) showed that the condensation of the intermediate components from the V phase to the L_1 phase occurred in the two-phase region ahead of the three-phase region. This condensation brought the L_1 phase closer to the L_2 phase at the leading edge of the three-phase region.

TABLE 4—BINARY INTERACTION PARAMETERS FOR THE HQ OIL

Components	PC1	PC2	PC3	PC4
PC1	0			
PC2	0.1000	0		
PC3	0.0100	0.0050	0	
PC4	0.1700	0.1400	0	0

We now explain the possibility that MCM is developed on an LCEP tie line for low-temperature CO_2 floods with the HQ oil. All flow simulations are performed with the UTCOMP simulator (Chang et al. 1990) with the conventional single-point upstream weighting scheme. The thermodynamic model used is the PR EOS. Viscosities are calculated with the method of Lohrenz et al. (1964), as implemented in UTCOMP.

It was challenging to create good simulation cases that satisfy the following: (1) Three phases are present in quaternary composition space at a low reservoir temperature; (2) three illustrative composition paths for fixed oil and gas compositions at three different pressures exhibit only LCEP, both LCEP and UCEP, and only two phases, respectively; and (3) simulations do not fail until at least 2.0 HCPVI. The search for the HQ quaternary fluid system **(Tables 3 and 4),** which was eventually found to be appropriate, began with the grouping of components in the 12-component SB oil model presented in Guler et al. (2001) (Tables 1 and 2). The reservoir temperature is 86°F for this oil. PC2 in the HQ system (Tables 3 and 4) was created by applying the mole-based mixing rule for a mixture of CO_2, C_1, C_2, C_3, nC_4, nC_5, and C_6. Similarly, PC3 and PC4 were created on the basis of a mixture of $C_{7–9}$, $C_{10–13}$, and $C_{14–19}$, and a mixture of $C_{20–35}$ and C_{36+}, respectively. PC1 in the HQ system is pure methane. The critical properties of PC1 taken from the PVTSim software (Calsep 2011) are only slightly different from those of C_1 in Guler et al. (2001) likely because they used different data sources. The oil and gas compositions and binary interaction parameters were adjusted further to satisfy the three requirements previously mentioned.

The P-T diagram for the HQ oil is given in **Fig. 1.** The bubble-point pressure is 1,694.63 psia at the reservoir temperature of 86°F. Three-phase equilibrium is observed at relatively low temperatures for the initial oil composition. Fig. 1 also presents the P-T envelope of the injection gas. The bubble- and dewpoints are 857.28 and 367.08 psia, respectively, at 86°F. The two-phase envelope of the injection gas exists near the vapor-pressure curve of pure CO_2.

Fig. 2 gives the P-x diagram for mixtures of the HQ oil and injection gas at 86°F. A four-hydrocarbon-phase region is observed at solvent mole fractions between 0.68 and 0.91 and pressures between 972 and 1,321 psia. They are the V, L_1, L_2, and a fourth hydrocarbon (L_3) phase. The L_3 phase is denser than the L_1 phase, and its viscosity is calculated to be approximately 10,000 cp at 1,000 psia and 86°F. The L_3 phase is not considered in all flow simulations in this research. In the P-x diagram, a wide three-hydrocarbon-phase region is present for the gas-mixing ratios higher than 20% within a reservoir-pressure range. Wide three-hydrocarbon-phase regions in P-x space were reported for Alaskan North Slope heavy oils and solvents in Okuyiga (1992), Godbole et al. (1995), McKean et al. (1999), Guler et al. (2001), and Wang et al. (2003). Because of the substantial upscaling performed in composition space for the HQ system, the three-hydrocarbon-phase region is calculated to be even wider than those

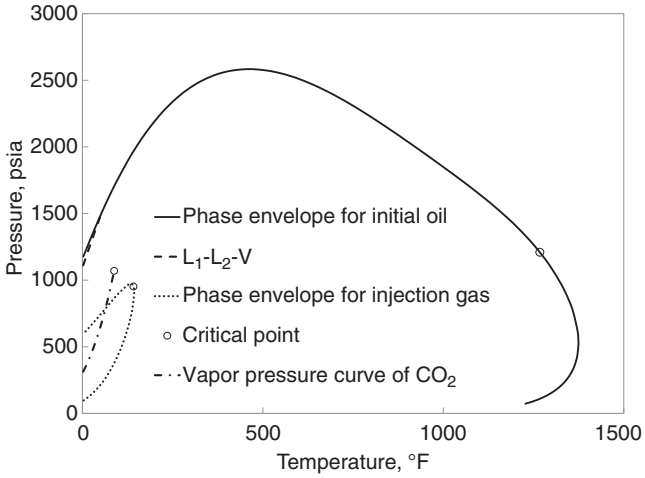

Fig. 1—The pressure-temperature (*P-T*) diagrams for the quaternary heavy (HQ) oil and injection gas given in Tables 3 and 4. The Peng-Robinson (PR) equation of state (EOS) is used. The saturation pressure of the oil is 1,694.63 psia at 86°F. Three-phase equilibrium is calculated at relatively low temperatures for the oleic (L_1), gaseous (V), and solvent-rich liquid (L_2) phases. The bubble- and dewpoints of the injection gas at 86°F are 857.28 psia and 367.08 psia, respectively.

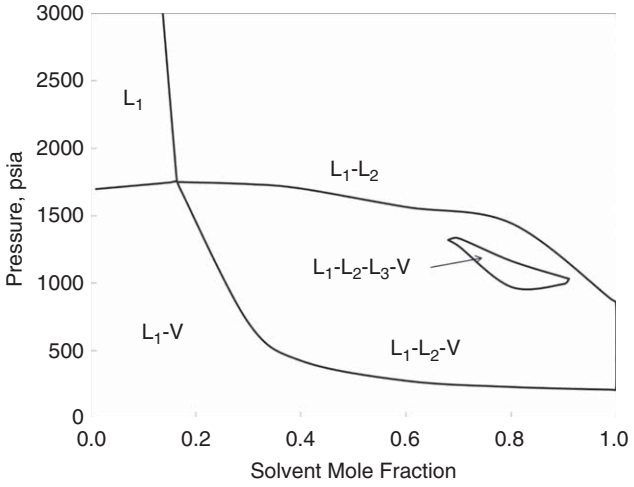

Fig. 2—Pressure-composition (*P-x*) diagram for mixtures of the HQ oil and injection gas given in Tables 3 and 4 at 86°F. A wide three-hydrocarbon-phase region is present for the gas-mixing ratios higher than 20% within a reservoir pressure range. The four-hydrocarbon-phase region consists of the V, L_1, L_2, and a fourth hydrocarbon (L_3) phases.

TABLE 5—RESERVOIR PROPERTIES FOR SIMULATIONS OF 1D OIL DISPLACEMENTS[a]

		Relative Permeability	Corey Model			
Dimensions	$10 \times 1 \times 10$ ft^3		W	L_1	V	L_2
Number of gridblocks	$1 \times 1{,}000 \times 1$	Residual saturation	0.40	0.20	0.05	0.05
Porosity	0.2	Endpoint relative permeability	0.35	0.50	0.65	0.65
Permeability	1,000 md	Exponent	3.0	3.0	3.0	3.0
		Initial saturation	0.4	0.6	0.0	0.0

[a]W: Aqueous phase, L_1: oleic phase, V: Gaseous phase, L_2: Solvent-rich liquid phase.

from experimental data and models with a larger number of components.

The injection gas is a binary mixture of PC1 and PC2, as given in Table 3. Its phase boundaries at 86°F can be found in Fig. 1. The mixing of a small amount of the oil with the injection gas at the temperature can exhibit the L_1-L_2, L_1-L_2-V or L_1-V equilibria, depending on pressures, as shown in Fig. 2. This also is shown later in quaternary diagrams at 1,000, 1,500, and 2,500 psia.

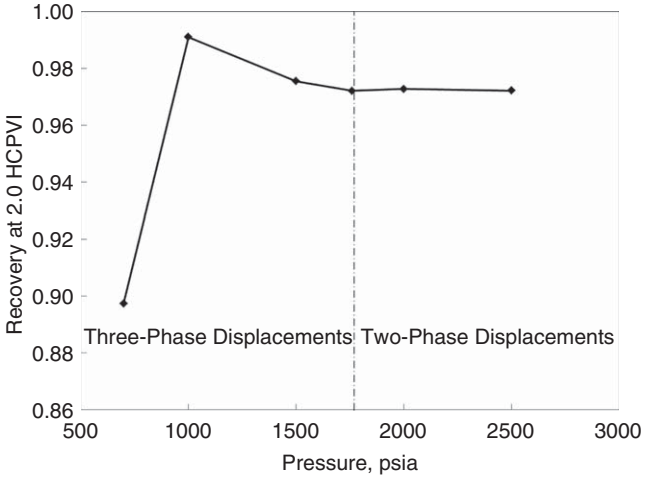

Fig. 3—HQ oil recoveries at 2.0 hydrocarbon-pore volume-injected (HCPVI) at 700, 1,000, 1,500, 1,700, 1,760, 2,000, and 2,500 psia. Reservoir and fluid properties are given in Tables 3 through 5. Three phases are observed for displacements at pressures up to 1,760 psia. The displacement at 1,000 psia yields 99.11% oil recovery at 2.0 HCPVI.

Table 5 shows the reservoir properties used in the flow simulations in this research. The relative permeabilities are based on the Corey model. The number of gridblocks is 1,000 in the displacement direction, and a uniform gridblock size of 1 ft is used. The initial water saturation is at the residual saturation of 0.4; water does not flow in all simulations in this study. Gas injection is continued until the trailing edge of the three-hydrocarbon-phase region reaches the outlet when three phases are present.

The HQ oil displacements are performed at 700, 1,000, 1,500, 1,700, 1,760, 2,000, and 2,500 psia. **Fig. 3** shows the oil recoveries at different pressures at 2.0 HCPVI. Oil recoveries at 1.5 HCPVI were also calculated, but nearly overlapped the values at 2.0 HCPVI in this case. Because of the volume-charging effect discussed in the Introduction section, all oil recoveries in this research are calculated at 2.0 HCPVI. This also keeps the consistency with oil-recovery calculation results presented in Okuno et al. (2011).

Three phases are observed for displacements at pressures up to 1,760 psia. At 700 psia, however, the oil recovery is low because propagation of the three-phase region is extremely slow. No three-phase equilibrium occurs in the displacements at 2,000 and 2,500 psia. Nearly perfect oil displacement is achieved at 1,000 psia, for which the oil recovery at 2.0 HCPVI is 99.11%. Although a small reduction of the recovery is observed for higher pressures as a result of numerical dispersion, their displacement efficiencies are still higher than 97% at 2.0 HCPVI. The main question to be addressed here is whether MCM is developed in these displacements.

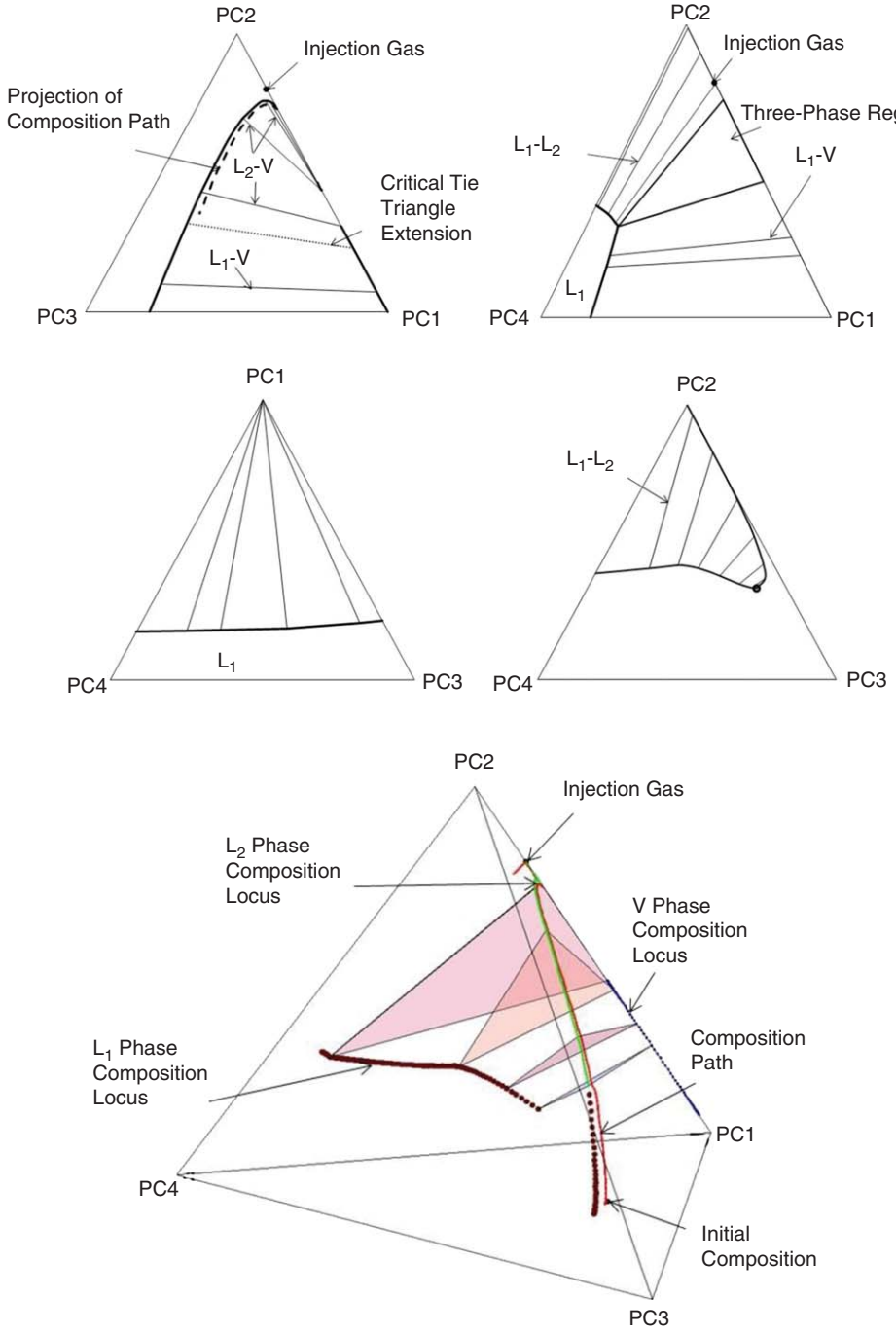

Fig. 4—Phase behavior along the composition path of the HQ oil displacement at 1,000 psia and 86°F. Phase behavior in the four ternary subsystems is presented in the top portion.

Fig. 4 presents phase behavior along the composition path in the quaternary diagram at 1,000 psia. Phase behavior in the four ternary subsystems is also given in the top portion of Fig. 4. The initial composition is in the L_1-V two-phase region because the saturation pressure is higher than 1,000 psia. Fig. 4 shows that the injection composition (20% PC1 and 80% PC2) forms the L_2 phase. This L_2 phase is an edge of an L_1-L_2 tie line in the quaternary diagram, as also confirmed in Fig. 2, in which the injection gas mixed with a small amount of the HQ oil forms the L_1-L_2 two phases at 1,000 psia.

Although three phases are observed along the composition path in the presence of numerical dispersion, the L_1 phase is essentially nonexistent upstream of the displacement front, as shown in **Fig. 5.** The leading edge of three phases is near the LCEP tie line, exhibiting an elongated tie triangle in Fig. 4. The LCEP is as follows: $L_1 = L_2$ at (0.1675, 0.2641, 0.5009, 0.0675) and V at (0.7784, 0.2216, 0.0000, 0.0000) in composition space. An approximate critical tie-triangle extension meets the PC1-PC2, PC2-PC3, PC3-PC4, and PC4-PC1 edges of the quaternary diagram at (0.7601, 0.2399, 0.000, 0.000), (0.000, 0.3422, 0.6578, 0.000), (0.000, 0.000, 0.3171, 0.6829), and (0.4335, 0.000, 0.000, 0.5665), respectively. This confirms that the initial composition is outside the critical tie-triangle extension, and it is possible to have a direct shock from the initial composition to the LCEP tie line. MCM can be developed on the LCEP tie line, as in the analytical solutions for the water and gas injection in LaForce and Orr (2008).

Fig. 6 shows the concentrations of the four components at 1,000 psia at 0.6 HCPVI. The concentration of PC4 decreases to be essentially zero at the three-phase leading edge; it is approximately 0.0025 from the dimensionless distance between 0.2 and 0.4 in Fig. 6. The PC4-free subsystem in Fig. 4 (top-left) shows

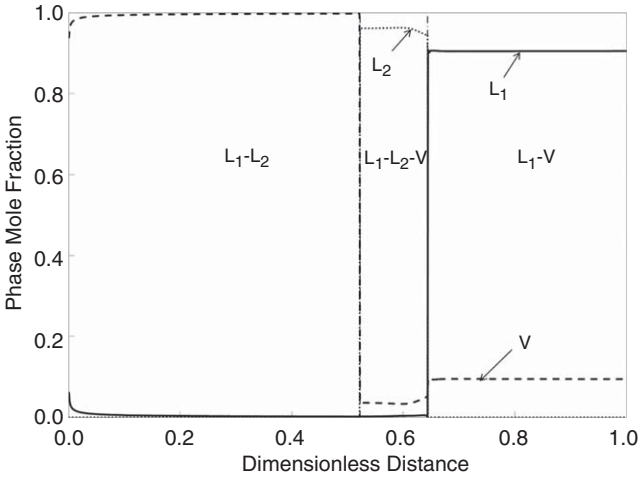

Fig. 5—Phase mole fractions for the HQ oil displacement at 1,000 psia and 86°F at 0.6 HCPVI. The L_1 phase is essentially nonexistent upstream of the displacement front.

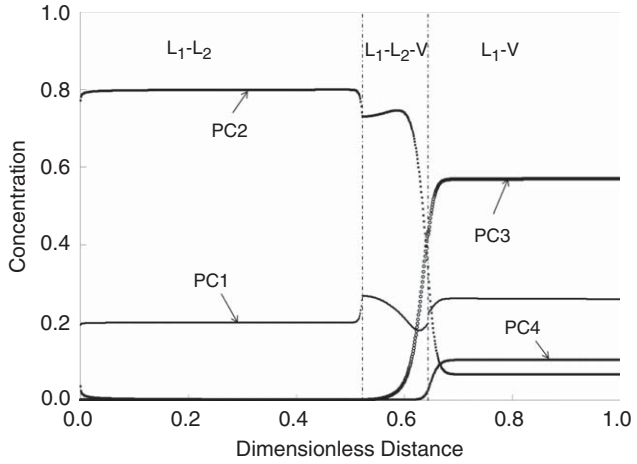

Fig. 6—Concentrations of the four components for the HQ oil displacement at 1,000 psia and 86°F at 0.6 HCPVI. The concentration of PC4 decreases to be essentially zero at the three-phase leading edge.

the projection of the composition path upstream of the three-phase leading edge as the dashed bold line. The intersection of the critical tie-triangle extension with this ternary subsystem is also shown as the dotted line. The equilibrium liquid phase in the two-phase region in this ternary subsystem is the L_2 phase above the critical tie-triangle extension. The equilibrium liquid phase below the critical tie-triangle extension is identified as the L_1 phase, considering that the PC1-PC3 binary subsystem shows the L_1-V two phases. That is, the L_1 phase is nonexistent upstream of the three-phase leading edge if the negligible amount of PC4 is not considered. The phase behavior in the PC4-free subsystem reconfirms that the L_1 phase is completely displaced by the L_2 phase on the LCEP for the limiting three-phase flow.

The HQ oil displacement at 1,500 psia yields 97.55% oil recovery at 2.0 HCPVI, as shown in Fig. 3. The three-phase region is detached from the PC3-free ternary subsystem, as shown in **Fig. 7.** The PC4-free ternary subsystem now has the L_2-V critical point, which is at equilibrium with the L_1 phase, forming the UCEP tie line in composition space. The initial composition is still in the L_1-V two-phase region. The phase mole fractions presented in **Fig. 8** show the formation of a gas bank ahead of the displacement front, which also can be seen in the composition path in Fig. 7.

The leading and trailing edges of the three-phase region show that the composition path is close to the LCEP and UCEP tie lines. The LCEP tie line is calculated as follows: $L_1 = L_2$ at (0.2389, 0.2096, 0.4775, 0.0740) and V at (0.8349, 0.1651, 0.0000, 0.0000) in composition space. An approximate critical tie-triangle extension meets the PC1-PC2, PC2-PC3, PC3-PC4, and PC4-PC1 edges of the quaternary diagram at (0.8349, 0.1651, 0.000, 0.000), (0.000, 0.3044, 0.6956, 0.000), (0.000, 0.000, 0.5899, 0.4101), and (0.7610, 0.000, 0.000, 0.2390), respectively. The initial composition is confirmed to be outside of the critical tie-triangle extension. Fig. 8 shows that the L_1 phase is essentially nonexistent upstream of the LCEP tie line, which is in line with **Fig. 9,** showing a negligible concentration of PC4 there at 1,500 psia at 0.6 HCPVI.

If the L_1 phase is completely displaced on the LCEP tie line for the limiting three-phase flow, the composition path upstream of the miscible front is on the PC4-free ternary subsystem. Fig. 7 (top-left) shows the projection of the composition path upstream of the LCEP tie line on the PC4-free ternary diagram as the dashed bold curve. The projected composition path traverses almost through the L_2-V critical point at (0.2338, 0.6904, 0.0757, 0.000). There is no multiphase region between the injection composition and the L_2-V critical point, as shown in Fig. 7 (top-left). Therefore, it is possible that single-phase flow occurs upstream of the miscible front on the LCEP tie line in the absence of numerical dispersion.

The HQ oil displacement at 2,500 psia results in 97.22% oil recovery at 2.0 HCPVI, as shown in Fig. 3. **Fig. 10** shows the composition path and two-phase behavior along the path. The initial composition is now a single-phase L_1 mixture. This is a typical vaporizing drive with converging K values in the displacement direction. A critical point for the L_1-L_2 two phases is at (0.3383, 0.3730, 0.2839, 0.0048) on the basis of the shortest tie line along the composition path. There is no multiphase region between this critical point and the initial composition. MCM is developed at the critical point as the limiting two-phase flow in the absence of numerical dispersion. **Figs. 11 and 12** show the phase mole fractions and components' concentrations at 2,500 psia at 0.6 HCPVI. Because of numerical dispersion, a small amount of the L_1 phase still exists, and the displacement of PC3 and PC4 is incomplete.

The results discussed previously indicate that MCM is likely developed in the HQ displacements at pressures more than 1,000 psia in the absence of dispersion. The effect of numerical dispersion seems to be less significant for the displacement at 1,000 psia than those at 1,500 and 2,500 psia. The effect of numerical dispersion on displacement efficiency, however, is not fully understood for three phases in the literature (LaForce and Orr 2009).

The gas bank ahead of three phases at 1,500 psia seems to accelerate the recoveries of PC3 and PC4 at early times (in HCPVI) in comparison with those in the displacement at 1,000 psia. For example, the PC3 recovery at 0.5 HCPVI is 48.32% at 1,000 psia and 50.70% at 1,500 psia. The PC4 recovery at 0.5 HCPVI is 48.35% at 1,000 psia and 50.95% at 1,500 psia. However, the comparison is not entirely clear because the two cases have different levels of numerical dispersion at different pressures.

The effect of the initial V phase saturation was studied on oil recovery with MCM developed through the conventional two-phase flow in LaForce and Johns (2010). They demonstrated that the initial V phase saturation delays oil recovery before the breakthrough of the miscible front, but does not affect development of MCM. Here, we show the effect of the initial V phase saturation on the HQ oil displacement at 1,000 psia. **Fig. 13** shows the composition paths for three different Initial Compositions A, B, and C, which are on the same tie line. Case A is the original case, shown in Fig. 4. Initial Compositions B and C are at (0.4460, 0.0635, 0.4148, 0.0757) and (0.6121, 0.0609, 0.2765, 0.0505), respectively. The three initial compositions are outside the critical tie-triangle extension, which is shown as a quadrilateral in Fig. 13.

Cases B and C form an oil bank resulting from the initial high mobility of the V phase. The three cases, however, give the same composition path upstream of Composition A. **Figs. 14–17** show the profiles of components' concentrations at 0.17 HCPVI for the

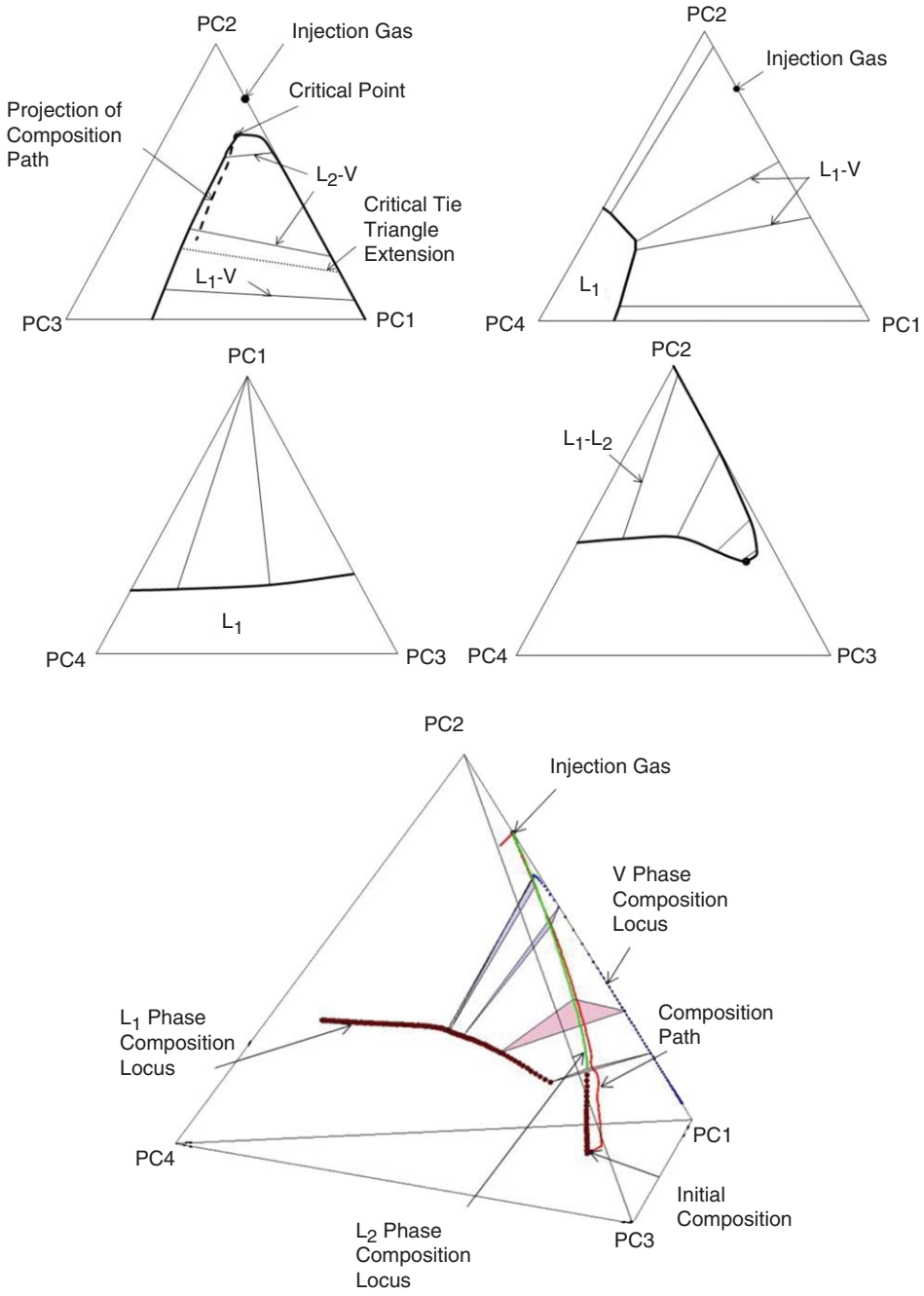

Fig. 7—Phase behavior along the composition path of the HQ oil displacement at 1,500 psia and 86°F. Phase behavior in the four ternary subsystems is presented in the top portion.

three cases. The formation of an oil bank can be seen in the profiles of PC3 and PC4 for Cases B and C. However, the profiles upstream of the miscible front are unaffected. **Figs. 18 and 19** present recoveries of PC3 and PC4, respectively. The PC4 recovery is normalized with the ultimate recovery for each case. This is because the PC4 recovery is less than 100% even at 2.0 HCPVI because of numerical dispersion, which can be observed as the small increase in the PC4 concentration near the inlet in Fig. 17. The delayed recovery of PC3 and PC4 is a direct result of the initial *V*-phase saturation. However, the development of MCM on the LCEP tie line is unaffected. These results are consistent with the results in LaForce and Johns (2005) presented for MCM through two-phase flow.

As previously shown, the interpretation of oil displacement by three hydrocarbon phases is complex even for 1D flow with no gravity (DeRuiter et al. 1994; Okuno and Xu 2014). When reservoir flow patterns of gas injection are concerned, one should take into account gravity segregation, front instability, and various crossflow mechanisms. Chang et al. (1994) and Chang (1990) presented a systematic investigation of reservoir flow patterns in CO_2 floods, such as viscous fingering, channeling, gravity override, and dispersive flow. Multidimensional numerical simulations of CO_2 floods were conducted with the UTCOMP simulator with a wide range of endpoint mobility ratio, gravity number, effective aspect ratio, longitudinal- and transverse-Peclet number, correlation length, and Dykstra-Parsons coefficient. They showed that viscous fingering was unlikely a dominant flow pattern for field-scale CO_2 flooding under secondary conditions without the use of water-alternating-gas injection, which would reduce the tendency of fingering. They concluded that fingering should be taken into account under typical laboratory conditions of low-effective-aspect ratio and low-permeability variation, but fingering would be much less likely to be important under reservoir conditions of a high-effective-aspect ratio. The dominant flow patterns were

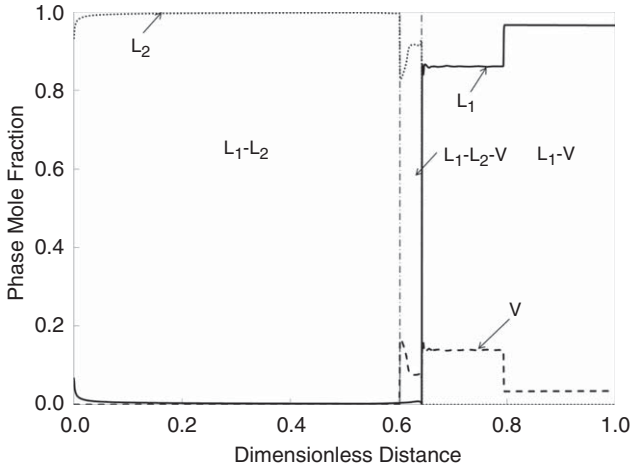

Fig. 8—Phase mole fractions for the HQ oil displacement at 1,500 psia and 86°F at 0.6 HCPVI. The L_1 phase is essentially nonexistent upstream of the displacement front. A gas bank is formed ahead of the displacement front, which also can be seen in the composition path in Fig. 7.

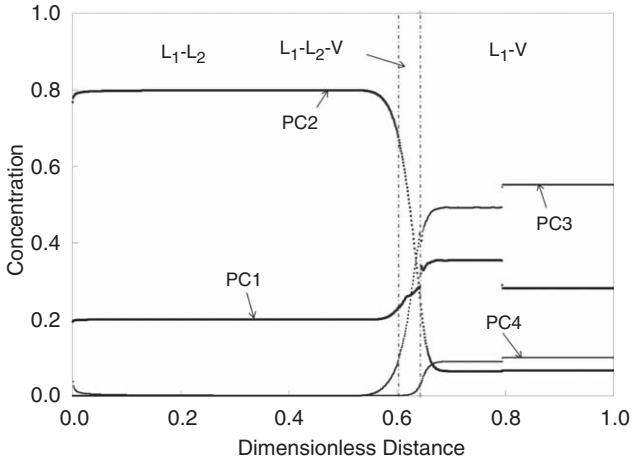

Fig. 9—Concentrations of the four components for the HQ oil displacement at 1,500 psia and 86°F at 0.6 HCPVI. The concentration of PC4 decreases to be essentially zero at the three-phase leading edge.

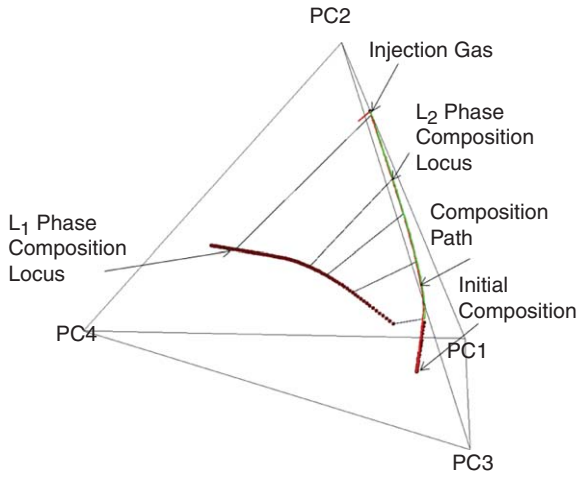

Fig. 10—Phase behavior along the composition path of the HQ oil displacement at 2,500 psia and 86°F. This is a typical vaporizing drive with converging *K* values in the displacement direction. Multicontact miscibility (MCM) is developed at the critical point as the limiting two-phase flow in the absence of numerical dispersion.

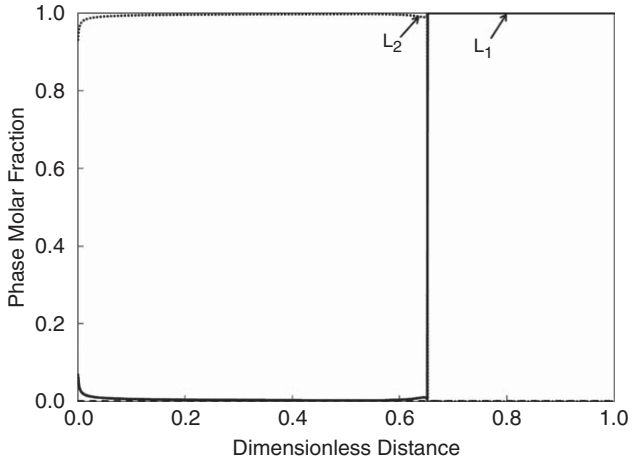

Fig. 11—Phase mole fractions for the HQ oil displacement at 2,500 psia and 86°F at 0.6 HCPVI.

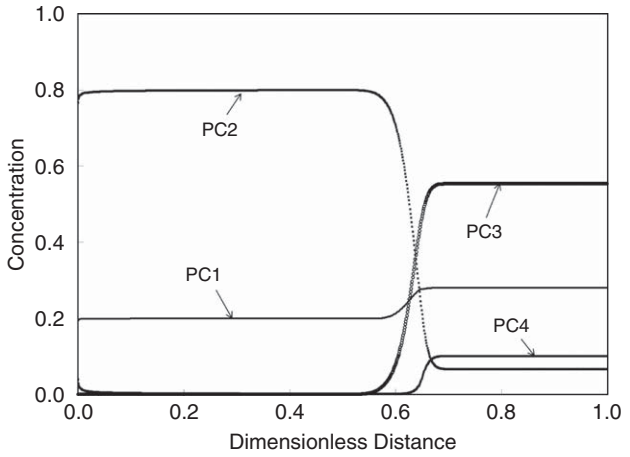

Fig. 12—Concentrations of the four components for the HQ oil displacement at 2,500 psia and 86°F at 0.6 HCPVI.

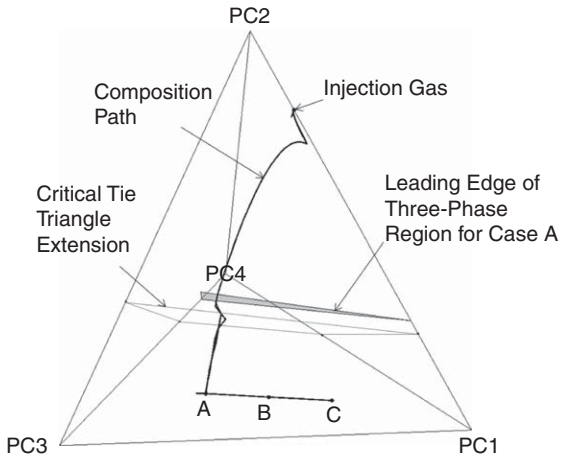

Fig. 13—Composition paths for three different Initial Compositions A, B, and C, which are on the same tie line. Case A is the original case shown in Fig. 4. Initial Compositions B and C are (0.4460, 0.0635, 0.4148, 0.0757) and (0.6121, 0.0609, 0.2765, 0.0505), respectively. The three initial compositions are outside the critical tie-triangle extension, which is shown as a dotted quadrilateral.

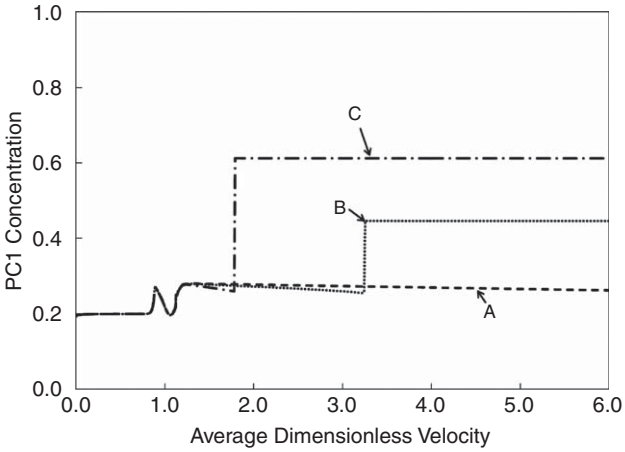

Fig. 14—Profiles of the PC1 concentrations at 0.17 HCPVI for Cases A, B, and C given in Fig. 13. The profiles are shown with the average velocity, the distance traveled divided by the hydrocarbon pore volumes injected.

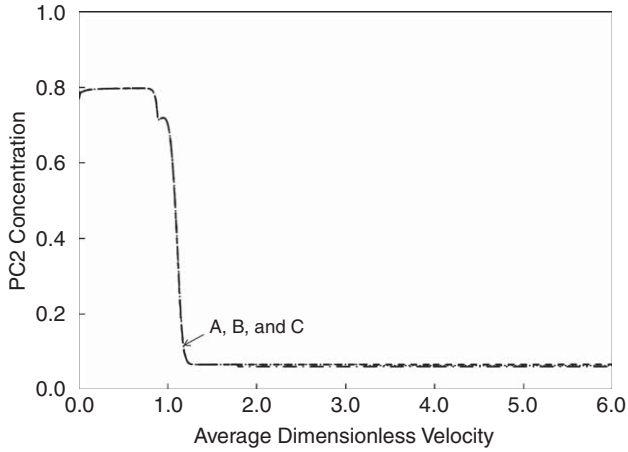

Fig. 15—Profiles of the PC2 concentrations at 0.17 HCPVI for Cases A, B, and C given in Fig. 13. The profiles are shown with the average velocity, the distance traveled divided by the hydrocarbon pore volumes injected.

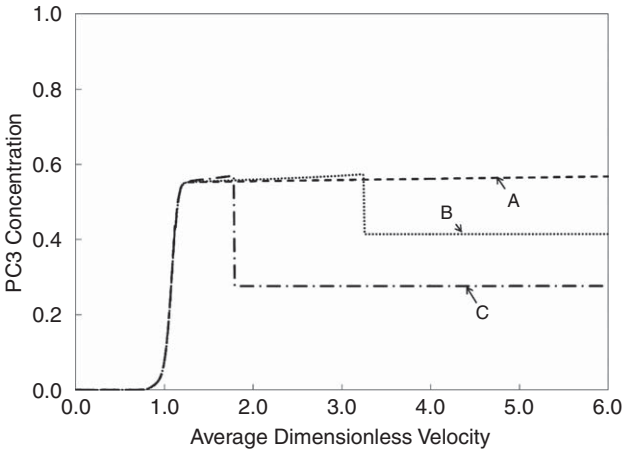

Fig. 16—Profiles of the PC3 concentrations at 0.17 HCPVI for Cases A, B, and C given in Fig. 13. The profiles are shown with the average velocity, the distance traveled divided by the hydrocarbon pore volumes injected.

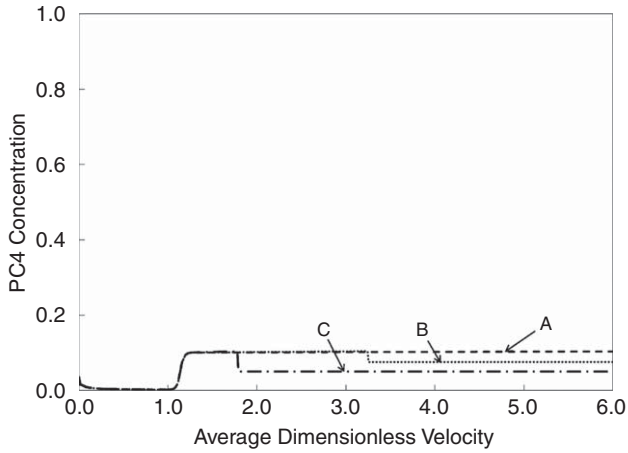

Fig. 17—Profiles of the PC4 concentrations at 0.17 HCPVI for Cases A, B, and C given in Fig. 13. The profiles are shown with the average velocity, the distance traveled divided by the hydrocarbon pore volumes injected.

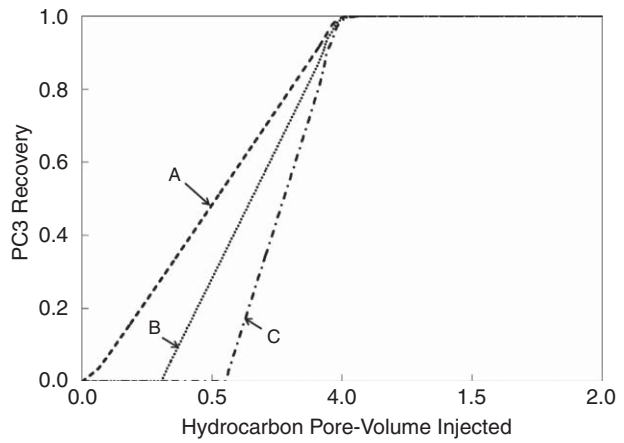

Fig. 18—PC3 recoveries for Cases A, B, and C given in Fig. 13. The recovery is delayed for Cases B and C because of the formation of the oil bank shown in Fig. 16.

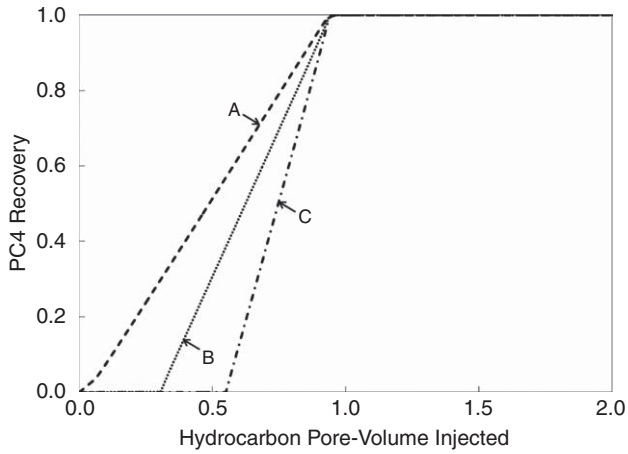

Fig. 19—PC4 recoveries for Cases A, B, and C given in Fig. 13. The PC4 recovery is normalized with the ultimate recovery for each case. The recovery is delayed for Cases B and C because of the formation of the oil bank shown in Fig. 17.

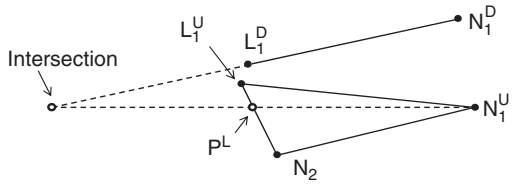

Fig. 20—Schematic of phase transition in composition space at the leading edge of the three-phase region. Black dots indicate equilibrium-phase compositions. Superscripts *D* and *U* represent downstream and upstream, respectively. Redistribution of components between two and three phases occurs through the intersection composition. The composition of the P^L pseudo phase is defined where the line connecting the intersection and the N_1^U phase composition meets (the extension of) the L_1-N_2 edge of the tie triangle.

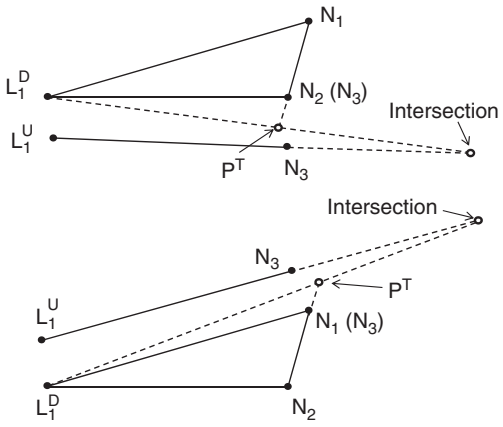

Fig. 21—Schematic of phase transition in composition space at the trailing edge of the three-phase region. Black dots indicate equilibrium phase compositions. Superscripts *D* and *U* represent downstream and upstream, respectively. Redistribution of components between two and three phases occurs through the intersection composition. The composition of the P^T pseudo phase is defined where the line connecting the intersection and the N_1^D phase composition meets the extension of the N_1-N_2 edge of the tie triangle. Two cases are possible, depending on the *N* phase that disappears at the trailing edge.

channeling, gravity override, and dispersive flow for most of the cases studied. The fluid model used was a ternary model of a Maljamar separator oil given by Ogino (1988). Three hydrocarbon phases were not predicted with this ternary fluid as presented in Chang (1990). The investigation by Tchelepi and Orr (1994) also suggested that channeling and gravity override would be dominant flow patterns if the reservoir was highly heterogeneous with large correlation lengths. To our knowledge, however, a similar investigation of reservoir flow patterns with three hydrocarbon phases is not yet presented in the literature.

Mass Transfer on Multiphase Transitions

Theory of gas injection is well-established to explain the interaction of flow in porous media with conventional two-hydrocarbon-phase behavior (Orr 2007). The interaction of flow with three hydrocarbon phases, however, is not fully understood. The main difference between two- and three-hydrocarbon-phase displacements is that the latter involves multiphase transitions between two and three phases (see Appendix B). Understanding of mass transfer among three hydrocarbon phases is important for the latter.

This section presents an analysis of mass conservation on multiphase transitions in three-hydrocarbon-phase displacements. The main objective is to investigate interphase mass transfer on multiphase transitions at the limit of three-phase flow. Conditions are derived for MCM development through three hydrocarbon phases. Quaternary cases are used to explain further these conditions.

Mass-conservation equations for 1D dispersion-free compositional flow are discretized in Appendix C for a multiphase transition between N_P^U and N_P^D phases, where N_P^U and N_P^D are the numbers of phases on the upstream and downstream sides, respectively. The resulting equation, Eq. C-6, is of the identical form with the generalized jump conditions that can be used in the MOC solution of multiphase flow (Okuno and Xu 2014). Appendix C presents that this equation can be used to analyze interphase mass transfer on multiphase transitions even in the presence of numerical dispersion.

Eq. C-6 states that a multiphase transition between N_P^U and N_P^D phases occurs through an intersection between the extensions of the two tie simplexes defined by $\underline{x}_j^U$ ($j=1, 2, \ldots, N_P^U$) and $\underline{x}_k^D$ ($k=1, 2, \ldots, N_P^D$), where $\underline{x}_j$ is the composition of equilibrium phase j. For a phase transition between one and two phases, this statement reduces to the well-known result of Helfferich (1981) that a shock between one and two phases must occur on the tie-line extension. A phase transition between two and three phases occurs through an intersection between the tie-line extension and the tie-triangle extension plane.

Figs. 20 and 21 show schematics for such phase transitions with the phase labeling in Fig. B-1. A pseudo phase P^L is defined in which the line connecting the intersection and the N_1^U phase composition meets (the extension of) the L_1-N_2 edge of the tie triangle. Redistribution of components from two to three phases can be considered to occur in three steps: (i) The L_1 and N_1 phases on the downstream tie line form the intersection composition; (ii) the intersection composition forms two phases, the P^L and N_1 phases, on the upstream tie triangle; and (iii) the P^L phase splits into the L_1 and N_2 phases on the tie triangle. A pseudo phase P^T is defined in which the line connecting the intersection and the L_1^D phase composition meets the extension of the N_1-N_2 edge of the tie triangle. The redistribution of components from three to two phases occurs in the following three steps: (i) The N_1 and N_2 phases form the P^T phase on the tie triangle extension downstream, (ii) the P^T and L_1 phases form the intersection composition, and (iii) the intersection composition forms the L_1 and N_3 phases on the tie line upstream. Fig. 21 shows two cases—one in which the N_1 phase disappears, and the other in which the N_2 phase disappears.

Efficient oil displacement by three hydrocarbon phases is possible when multiphase transitions at the leading and trailing edges of the three-phase region occur in the way described in Okuno et al. (2011). Thus, at the leading edge of the three-phase region, the L_1^D phase should split into the L_1^U and N_2^U phases without affecting the N_1 phase. Also, at the trailing edge of the three-phase region, the N_1^U and N_2^U phases should merge into the N_3 phase without affecting the L_1 phase. Mathematical expressions for these ideal phase transitions are $\delta^L=0$ for the leading edge and $\delta^T=0$ for the trailing edge of the three-phase region, where

$$\delta^L = \| \Gamma_{N_1}^U \underline{x}_{N_1}^U - \Gamma_{N_1}^D \underline{x}_{N_1}^D \|_2 \quad \ldots\ldots\ldots\ldots\ldots\ldots (1)$$

$$\delta^T = \| \Gamma_{L_1}^U \underline{x}_{L_1}^U - \Gamma_{L_1}^D \underline{x}_{L_1}^D \|_2. \quad \ldots\ldots\ldots\ldots\ldots\ldots (2)$$

These distance parameters were derived and used to quantify the efficiency of heavy-oil displacements by three hydrocarbon phases in Okuno and Xu (2014).

In this paper, we consider further the necessary and sufficient conditions for the ideal multiphase transitions. Thus, $\delta\underline{x}^L = \delta\Gamma^L = 0$ are the necessary and sufficient conditions for δ^L to be zero, where

$$\delta\underline{x}^L = \| \underline{x}_{N_1}^U - \underline{x}_{N_1}^D \|_2 \quad \ldots\ldots\ldots\ldots\ldots\ldots\ldots\ldots (3)$$

and

$$\delta\Gamma^L = |\Gamma_{N_1}^U - \Gamma_{N_1}^D|. \quad \ldots\ldots\ldots\ldots\ldots\ldots\ldots\ldots (4)$$

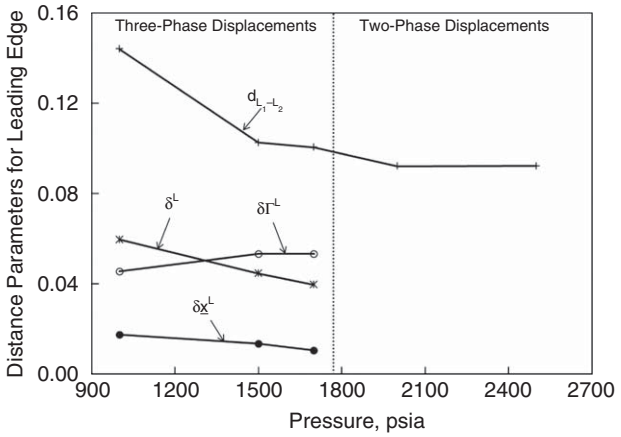

Fig. 22—Distance parameters for the leading edge for the HQ oil displacements at 86°F. Reservoir and fluid properties are given in Tables 3, 4, and 5.

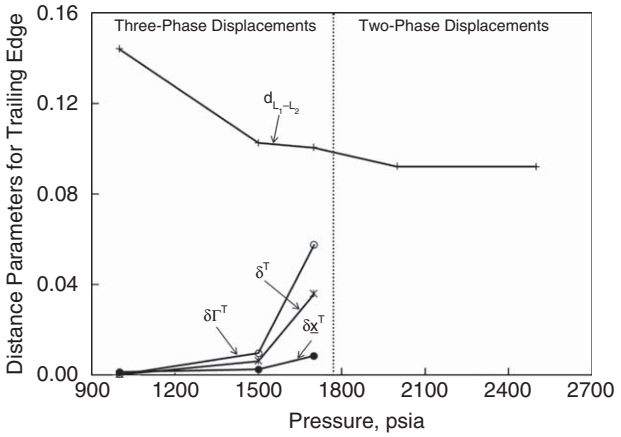

Fig. 23—Distance parameters for the trailing edge for the HQ oil displacements at 86°F. Reservoir and fluid properties are given in Tables 3, 4, and 5.

These conditions are simultaneously satisfied when the N_1-P^L pseudo tie line coincides with the N_1-L_1 tie line (see Fig. 20). For this ideal case, the phase transition would occur either on the N_1-L_1 edge of the tie triangle or on the LCEP tie line.

Similarly, $\delta\underline{x}^T = \delta\Gamma^T = 0$ are the necessary and sufficient conditions for δ^T to be zero, where

$$\delta\underline{x}^T = \| \underline{x}^U_{L_1} - \underline{x}^D_{L_1} \|_2 \quad \ldots\ldots\ldots\ldots\ldots\ldots\ldots\ldots\ldots\ldots (5)$$

and

$$\delta\Gamma^T = |\Gamma^U_{L_1} - \Gamma^D_{L_1}| . \quad \ldots\ldots\ldots\ldots\ldots\ldots\ldots\ldots\ldots\ldots (6)$$

This ideal phase transition would occur either on the L_1-N_3 edge of the tie triangle or on the UCEP tie line, at which the L_1-P^T pseudo tie line coincides with the L_1-N_3 tie line (see Fig. 21).

Analytical solutions of 1D dispersion-free compositional flow show that a composition shock is generally required on a phase transition (Orr 2007; LaForce et al. 2008b; LaForce and Orr 2008). LaForce and Orr (2009), however, presented analytical solutions for oil displacements that cross the boundary between two and three phases without a shock on the basis of the Corey relative permeabilities. The distance (δ) parameter will be zero for this type of continuous phase transition because it occurs on a tie-triangle edge.

The previous section presented that three-hydrocarbon-phase flow can develop MCM on the LCEP tie line, in which the non-V phase switches its identity from L_1 to L_2 with no three-phase equilibrium involved. When this occurs at the leading edge of three phases, $d_{L1\text{-}L2}$, $\delta\underline{x}^L$, $\delta\Gamma^L$, and δ^L are all zero. Then, the L_1 phase must be nonexistent at the trailing edge of three phases for this limiting case because the L_1 phase is completely displaced by the L_2 phase on the LCEP tie line. Therefore, the ideal phase transition at the trailing edge given in Eqs. 5 and 6 must occur with the overall composition on the N_3 edge of the L_1-N_3 tie line (see Fig. 21). Thus, at the limit of three-phase displacements, the interphase mass transfer occurs in the ideal manner: $\delta^L = \delta^T = 0$. This is analogous to MCM development in the traditional two-phase displacements; the single-phase flow changes its identities from L_1 to V at the displacement front at the limit of two-phase displacements when any one of the key tie lines becomes a critical tie line (Johns 1992).

The preceding discussion combines the new analysis of the mass conservation on multiphase transition in this research with recent analytical research on three-phase displacements by LaForce and Orr (2008, 2009) and LaForce (2012). The main point made here is that MCM development on the LCEP tie line for the limiting three-phase displacement must satisfy the following conditions: $d_{L1\text{-}L2} = \delta\underline{x}^L = \delta\Gamma^L = \delta^L = 0.0$ at the leading edge of three phases, and $\delta\underline{x}^T = \delta\Gamma^T = \delta^T = 0.0$ at the trailing edge of three phases. Note that the criticality condition for UCEP ($d_{V\text{-}L2} = 0$) is not considered here because it is not directly related to miscibility with the L_1 phase, although it likely affects flow.

The most fundamental condition $d_{L1\text{-}L2} = 0.0$, however, was unsuccessful in indicating MCM development because of a significant numerical dispersion at the leading edge of three phases in Okuno et al. (2011), as described in the Introduction section. An MCM composition path that otherwise would traverse along phase boundaries (e.g., an edge of a CEP or a vertex of a tie triangle) can go just inside a multiphase region in the presence of numerical dispersion, resulting in positive values for the distance parameters.

The distance parameters are calculated for the HQ oil displacements. The distance parameters for the leading edge, $d_{L1\text{-}L2}$, $\delta\underline{x}^L$, $\delta\Gamma^L$, and δ^L, are presented in **Fig. 22** for two- and three-phase displacements of the HQ oil. The compositions near the three-phase leading edge are affected significantly by numerical dispersion because components' concentrations drastically change there, as shown in Fig. 6. As expected, the $d_{L1\text{-}L2}$ parameter is not a good indicator for the development of MCM through three phases in these simulations. The mass-transfer-related parameters, $\delta\underline{x}^L$, $\delta\Gamma^L$, and δ^L, are nearly constant with pressure at the leading edge. The positive values presented in Fig. 22 for $d_{L1\text{-}L2}$, $\delta\underline{x}^L$, $\delta\Gamma^L$, and δ^L indicate imperfect oil displacement at the leading edge in the presence of numerical dispersion.

The distance parameters for the trailing edge, $\delta\underline{x}^T$, $\delta\,\Gamma^T$, and δ^T, are presented in **Fig. 23.** Mass transfer at the trailing edge becomes more favorable as pressure decreases. At 1,000 psia, $\delta\underline{x}^T$ and $\delta\Gamma^T$ are 1.2×10^{-3} and 1.0×10^{-4}, respectively, resulting in δ^T of 5.0×10^{-5}. The mole fraction of the L_1 phase at the trailing edge is 0.002 at this pressure (i.e., the L_1 phase is nearly nonexistent). This indicates that 1,000 psia is close to the MMP for the HQ oil displacement studied here. Fig. 3 shows the highest oil recovery of 99.11% at 1,000 psia at 2.0 HCPVI. Even though the distance parameters at the trailing edge indicate that the MCM conditions are nearly satisfied, three-phase flow occurs because of numerical dispersion, especially near the displacement front.

Figs. 22 and 23 also show how the transition occurs between two- and three-phase displacements. The increasing trend of δ^T with respect to pressure indicates that mass transfer at the trailing edge becomes less favorable for oil recovery with increasing pressure. During this pressure increase, the three-phase region gradually shrinks until it disappears at approximately 1,760 psia in the simulations. At pressures more than 1,760 psia, only two liquid phases (i.e., L_1 and L_2) are present in the displacements. The transition from three- to two-phase displacement occurs as interphase mass transfer at the trailing edge gradually deviates from the best possible way; $\delta^L = \delta^L = 0$ (see Eqs. 1 and 2). The $d_{L1\text{-}L2}$ parameter gradually decreases with increasing pressure. However, the $d_{L1\text{-}L2}$ value is still 0.0919 at 2,500 psia. The MCM conditions for the leading edge tend to be affected significantly by the numerical dispersion.

TABLE 6—EOS PARAMETERS FOR THE BOB SLAUGHTER BLOCK OIL (KHAN ET AL. 1992)

Components	Oil (Mole %)	Gas (Mole %)	Molecular Weight	*Tc* (°R)	*Pc* (psia)	*Vc* (ft^3/lb-mol)	Acentric Factor	BIC* CO_2
CO_2	3.37	95.0	44.01	547.56	1,069.87	1.506	0.2250	0.000
C_1	8.61	5.0	16.04	288.00	667.20	1.586	0.0080	0.055
C_{2-3}	15.03	0.0	37.20	619.57	652.56	2.902	0.1305	0.055
C_{4-6}	16.71	0.0	69.50	833.80	493.07	4.914	0.1404	0.055
C_{7-15}	33.04	0.0	140.96	1090.35	315.44	9.000	0.6177	0.105
C_{16-27}	16.11	0.0	280.99	1351.83	239.90	17.100	0.9566	0.105
C_{28+}	7.13	0.0	519.62	1694.46	238.12	32.500	1.2683	0.105

*BIC = binary interaction coefficients.

Results of the HQ-oil displacement simulations indicate that the effect of dispersion on three-phase flow may be different from that on two-phase flow. Johns et al. (2000) showed that gas enrichment greater than the minimal miscibility enrichment can enhance the local displacement efficiency in *L-V* two-phase flow under dispersion. Fig. 3, however, presents that the displacement efficiency of three-phase-flow decreases as the miscibility level is increased above the MMP (approximately 1,000 psia). We have explained that this decreasing trend of three-phase displacement efficiency comes from the decreasing efficiency of the interphase mass transfer on multiphase transitions. However, it is uncertain how dispersion affects the interphase mass transfer on multiphase transitions (i.e., the leading and trailing edges of three phases). Further investigation of dispersion effects on three-phase flow is necessary.

As discussed in the Introduction section, Okuno and Xu (2014) presented quaternary oil displacements that exhibit a nonmonotonic trend of oil recovery at a throughput with respect to gas enrichment and pressure. We have confirmed that the initial oil composition existed inside the critical tie-triangle extension planes at the pressures considered in their quaternary displacements for a fixed injection gas and oil. Thus, these quaternary displacements in Okuno and Xu (2014) could not have a direct shock onto the LCEP from the initial oil composition, unlike the HQ case presented previously. In both quaternary cases, however, the δ^T parameter increased as pressure was increased above an optimum, resulting in less-efficient three-phase displacement. The increasing trend of δ^T with pressure in the HQ case may be associated with the dispersion effects, as discussed in the previous paragraph. In the quaternary displacements in Okuno and Xu (2014), it also may be because the level of miscibility decreased as pressure was increased above an optimum. This possibility was indicated in our calculation result that the initial oil composition used in Okuno and Xu (2014) became deeper inside the critical tie-triangle extension plane as pressure was increased above the optimum. To recap, the interphase mass transfer successfully represented the three-phase displacement efficiency in both quaternary cases, although various factors affected the local displacement efficiency of three phases, such as the levels of dispersion and miscibility.

Case Studies

In this section, the MCM conditions are applied to 1D CO_2 floods for the Bob Slaughter Block and SB oils. The former is a west-Texas oil, and the latter is an Alaskan heavy oil. The reservoir properties commonly used are given in Table 5. The objective of this section is to confirm the MCM conditions derived in the previous section in multicomponent oil displacements.

Bob Slaughter Block Oil Displacement. The Bob Slaughter Block fluid model developed by Khan et al. (1992) is used, as presented in **Table 6.** The injection gas consists of 95% CO_2 and 5% methane, as used in Okuno et al. (2011). The reservoir temperature is 105°F. Oil displacements are simulated at 1,150, 1,250, 1,350, 1,400, 1,500, 1.600, and 1,750 psia. Three phases are present in all these displacements. Details of phase behavior for these displacements are given in Okuno (2009) and Okuno et al. (2011), and not duplicated here.

Oil recovery at a given throughput monotonically increases with pressure, as presented in **Fig. 24.** The displacement at 1,750 psia achieves the efficiency of 97.22% at 2.0 HCPVI. **Figs. 25 and 26** show the distance parameters calculated for the leading and trailing edges of three phases, respectively. The parameters for the leading edge are affected by numerical dispersion as mentioned in the previous section. The development of MCM through

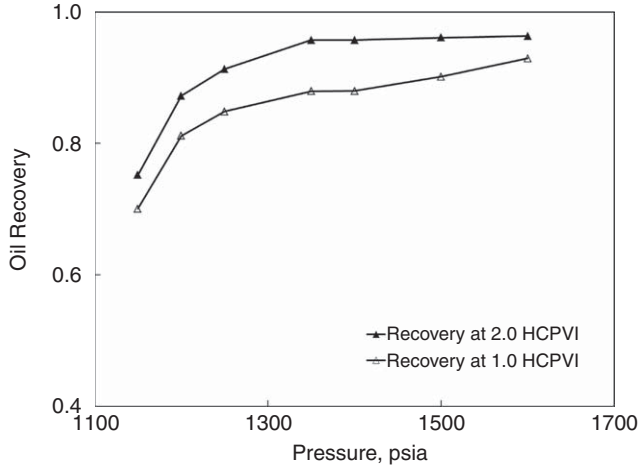

Fig. 24—Oil recoveries for the Bob Slaughter Block oil displacements at different pressures at 105°F. Reservoir and fluid properties are given in Tables 5 and 6, respectively.

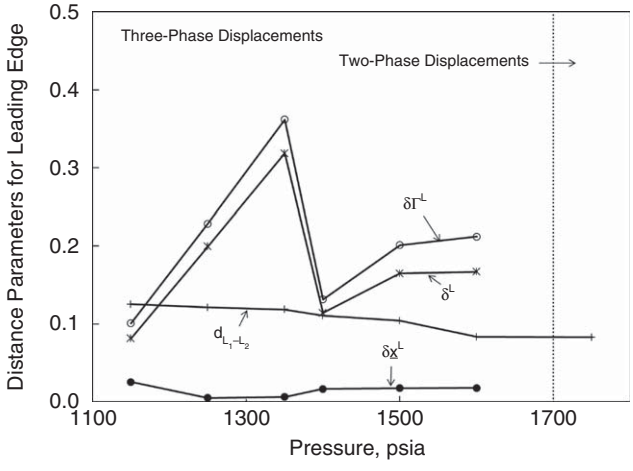

Fig. 25—Distance parameters for the leading edge for the Bob Slaughter Block oil displacements at 105°F. Reservoir and fluid properties are given in Tables 5 and 6, respectively.

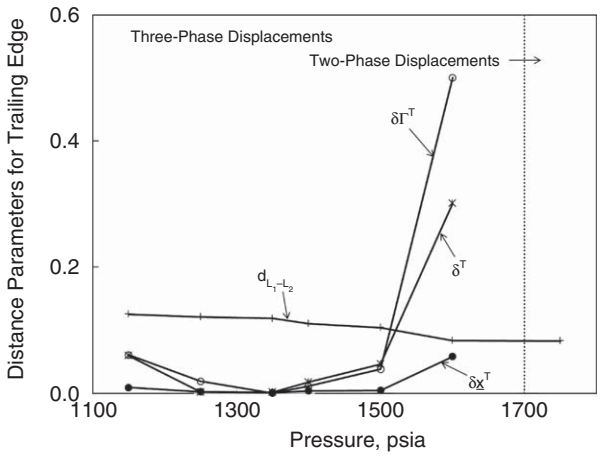

Fig. 26—Distance parameters for the trailing edge for the Bob Slaughter Block oil displacements at 105°F. Reservoir and fluid properties are given in Tables 5 and 6, respectively.

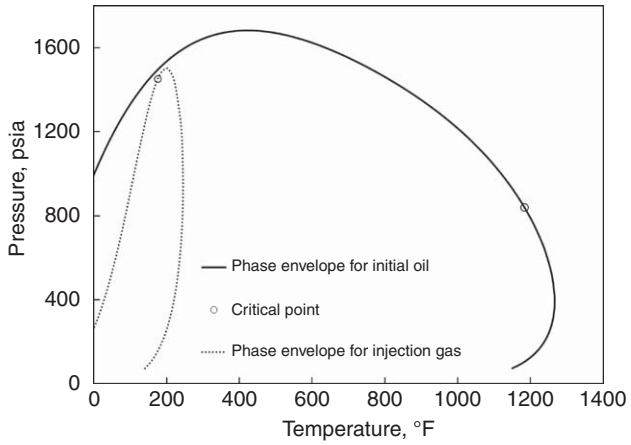

Fig. 27—*P-T* diagrams for the Schrader Bluff (SB) oil and the injection gas on the basis of the PR EOS fluid model developed by Guler et al. (2001). The parameters are given in Tables 1 and 2. The saturation pressure of the oil is 1292.7 psia at 86°F.

three phases is clear neither from the proximity measure for LCEP ($d_{L1\text{-}L2}$) nor from the mass transfer (δ^L). The $\delta \underline{x}^T$, $\delta\Gamma^T$, and δ^T parameters in Fig. 26 show that mass transfer at the trailing edge becomes most favorable at 1,350 psia. At this pressure, $\delta \underline{x}^T$ is 7.9×10^{-4}, and $\delta\Gamma^T$ is 2.0×10^{-4}, resulting in δ^T of 1.5×10^{-3}. MCM development through three phases likely occurs near this pressure on the basis of these simulations.

Fig. 26 also presents the transition from three- to two-phase displacements as pressure increases. As mentioned previously, interphase mass transfer is most favorable at 1,350 psia, and gradually becomes unfavorable with increasing pressure. At pressures greater than 1,350 psia, two-phase flow dominates the displacement process over the three-phase flow. In this transition process, the three-phase region shrinks and finally disappears. Three phases are not present at 1,750 psia.

SB Oil Displacement. The EOS model developed by Guler et al. (2001) is used, as shown in Tables 1 and 2. The injection gas consists of 81.5% CO_2, 0.43% C_3, 7.98% n-C_4, 5.22% n-C_5, 2.67% n-C_6, and 2.20% C_{7-9}. **Fig. 27** shows the *P-T* diagram for the oil and injection gas. The saturation pressure at the reservoir temperature of 86°F is 1,292.7 psia. **Fig. 28** gives the *P-x* diagram for the oil and injection gas at 86°F, which presents a large three-phase region for a wide pressure range.

Fig. 29 shows the oil recoveries at 600, 800, 1,000, 1,500, 1,800, 2,500, 3,500, and 4,000 psia. Three phases are present for all the displacements except for those at pressures 3,500 and 4,000 psia. The propagation of three phases is extremely slow at 600 psia, resulting in an inefficient displacement of oil. The oil recovery at 2.0 HCPVI exhibits the maximum of 99.99% at 800 psia. As the pressure increases, the oil recovery first decreases to 96.40% at 2,500 psia, and then increases to 98.13% at 3,500 psia. The displacements are controlled by L_1-L_2 two-phase flow at 3,500 and 4,000 psia.

The distance parameters for the trailing edge, $\delta \underline{x}^T$, $\delta\Gamma^T$, and δ^T, clearly show the possibility that MCM through three phases is developed near 800 psia, as shown in **Fig. 30.** The L_1 phase mole fraction at the trailing edge is 0.002 at 800 psia (i.e., the displacement of the L_1 phase is nearly complete).

The distance parameters for the leading edge, $d_{L1\text{-}L2}$, $\delta \underline{x}^L$, $\delta\Gamma^L$, and δ^L, are presented in **Fig. 31.** The composition path traverses closer to the LCEP tie line as pressure increases because the $d_{L1\text{-}L2}$ parameter monotonically decreases with increasing pressure. However, the mass-transfer-related parameters $\delta \underline{x}^L$, $\delta\Gamma^L$, and δ^L indicate that the multiphase transition becomes less favorable in terms of oil recovery with increasing pressure. The transition from three- to two-phase flow gradually occurs. This transition from three- to two-phase flow likely explains the nonmonotonic recovery at a given throughput presented in Fig. 29 because the effects of dispersion are different for two- and three-phase flows.

We also applied the MCM conditions derived in this research to other low-temperature CO_2 flooding simulations, such as the BSB-Q, North Ward Estes, Oil G, and Monahans Clearfork displacements (Khan et al. 1992; Lim et al. 1992; Okuno et al. 2011). The cases studied showed that the MCM conditions for the

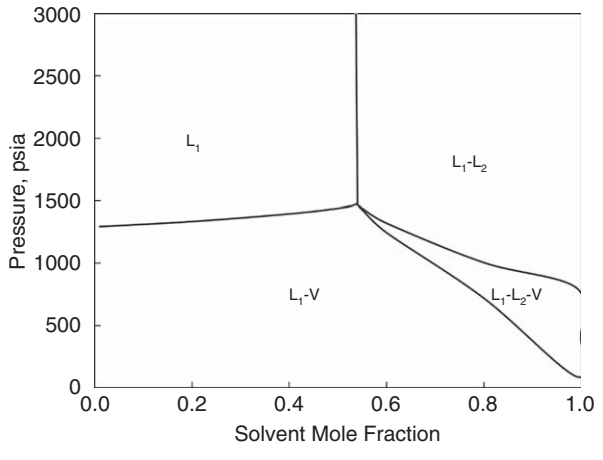

Fig. 28—*P-x* diagram for the oil and injection gas at 86°F. The oil and gas properties are presented in Tables 1 and 2.

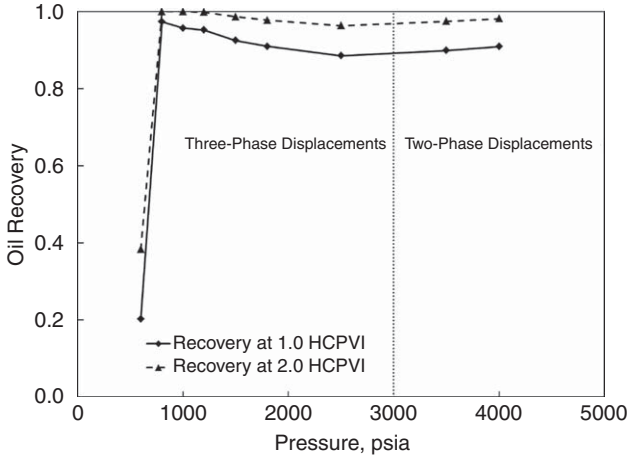

Fig. 29—Oil recoveries for the SB oil displacements at different pressures at 86°F. Reservoir properties and fluid properties are given in Tables 5, 1, and 2, respectively.

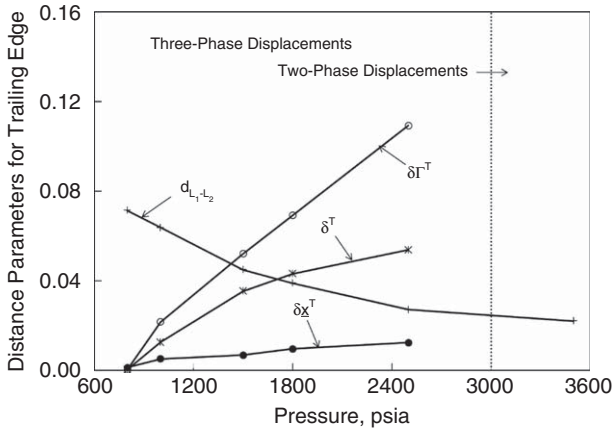

Fig. 30—Distance parameters for the trailing edge for the SB oil displacements at 86°F. Reservoir and fluid properties are given in Tables 5, 1, and 2, respectively.

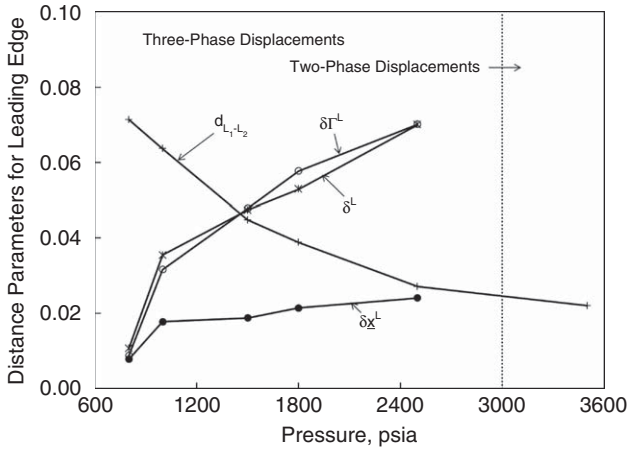

Fig. 31—Distance parameters for the leading edge for the SB oil displacements at 86°F. Reservoir and fluid properties are given in Tables 5, 1, and 2, respectively.

leading edge can be significantly affected by numerical dispersion. It was observed consistently in these simulations that the MCM conditions $\delta\underline{x}^T = \delta\Gamma^T = \delta^T = 0.0$ at the trailing edge of three phases are clearly correlated to the oil-displacement efficiency by three hydrocarbon phases.

Conclusions

This paper presented a detailed analysis of mass conservation on multiphase transitions in low-temperature CO_2 floods. The main focus of the analysis was on interphase mass transfer when MCM is developed for the limiting three-hydrocarbon-phase displacement. Simple analytical conditions were derived for MCM through three phases. Case studies were conducted to show applications of the derived MCM conditions to oil displacements with four and more components. Conclusions are as follows:

- MCM in three-hydrocarbon-phase displacements can be developed on an LCEP tie line, in which the oleic (L_1) phase is completely displaced by the solvent-rich (L_2) liquid phase in the presence of the gaseous (V) phase. This MCM development can be interpreted as the limiting three-phase flow on the boundary between two- and three-phase flow, which is analogous to analytical solutions of water and gas injection presented in LaForce and Orr (2008, 2009). Two non-L_1 phases are present upstream of the miscible front, that is, L_2 and V in three-hydrocarbon-phase flow in this research, and the aqueous (W) and V phases in water and gas injection of LaForce and Orr (2008, 2009). The L_2 and V phases also can be miscible at the UCEP, resulting in single-phase flow upstream of the miscible front.
- Simulations were conducted for different initial V-phase saturations for MCM flow through three phases. The presence of the initial V phase can delay the oil recovery before breakthrough of the miscible front. This is consistent with results of LaForce and Johns (2005), who studied the effect of initial gas saturation on miscible flow developed through the conventional V-L two phases. The initial V-phase saturation did not affect MCM development on an LCEP in the cases studied.
- Interphase mass transfer was analyzed by considering mass conservation for multiphase transitions between two and three phases. We presented the necessary and sufficient conditions for the best-possible multiphase transitions in terms of oil-displacement efficiency (Eqs. 1 through 6). These conditions must be satisfied on MCM development through three hydrocarbon phases. Simulation cases showed that they are nearly satisfied when the effect of numerical dispersion is small. MCM is likely developed through three hydrocarbon phases on the LCEP in the cases studied.
- Three-phase flow gradually changes to two-phase flow with varying thermodynamic conditions in the presence of dispersion. During the change, interphase mass transfer gradually deviates from the best-possible way described with Eqs. 1 through 6. The three-phase region shrinks until it disappears, resulting in a two-phase displacement.
- The interphase mass transfer successfully represented the three-phase displacement efficiency in the cases studied in the current paper and Okuno and Xu (2014). Various factors affected the displacement efficiency of three phases, such as the levels of dispersion and miscibility. Further investigation is necessary into the dispersion effect on the interphase mass transfer on multiphase transitions at the leading and trailing edges of three phases.

Nomenclature

c_{ij} = volumetric fraction of component i in phase j
$\underline{c}_j$ = vector consisting of c_{ij} as defined in Eq. C-4
C_i = overall volume fraction of component i
d = distance between two equilibrium-phase compositions x
f_j = fractional flow of phase j
F_i = overall fractional flow of component i
L_1 = oleic phase
L_2 = solvent-rich liquid phase
N_C = number of components
N_j (j =1, 2, or 3) = nonoleic phase (i.e., L_2 or V)
N_P = number of phases
P = pressure or pseudo phase
P_C = critical pressure
S_j = saturation of phase j
T = temperature
T_C = critical temperature
t_D = dimensionless time in pore volumes
V = gaseous phase
V_C = critical volume
v_D = dimensionless velocity of phase transition defined in Eq. C-3
W = aqueous phase
$\underline{x}$ = composition
x_D = dimensionless distance from the injector
x_{ij} = mole fraction of component i in phase j
$\underline{x}_j$ = vector consisting of x_{ij}
$\underline{z}$ = overall composition vector

Superscripts

D = downstream
L = leading edge of three phases
T = trailing edge of three phases
U = upstream
γ = parameter defined in Eq. C-5
Γ = parameter defined in Eq. C-6

δ = distance defined in Eqs. 1 and 2
Λ = dimensionless shock velocity

Acknowledgments

This research was funded by research grants from the Natural Sciences and Engineering Research Council of Canada (RGPIN 418266) and Japan Petroleum Exploration Company, Limited (JAPEX). Ryosuke Okuno was awarded the SPE Petroleum Engineering Junior Faculty Research Initiation Award. Zhongguo Xu has received a scholarship from the China Scholarship Council. We gratefully acknowledge these supports. We also thank Dr. Kamy Sepehrnoori for providing the UTCOMP simulator. Flow simulations in this research were conducted by use of the computational facility of Compute Canada.

References

Ahmadi, K. 2011. *Advances in Calculation of Minimum Miscibility Pressure*. PhD dissertation, University of Texas at Austin, Austin, Texas (May 2011).

Ahmadi, K. and Johns, R.T. 2011. Multiple Mixing-Cell Method for MMP Calculations. *SPE J.* **16** (4): 733–742. http://dx.doi.org/10.2118/116823-PA.

Bluma, M. and Deiters, U.K. 1999. A Classification of Phase Diagrams of Ternary Fluid Systems. *Physical Chemistry Chemical Physics* **1** (18): 4307–4313.

Chang. Y.-B. 1990. *Development and Application of an Equation of State Compositional Simulator*. PhD dissertation, University of Texas at Austin, Austin, Texas (August 1990).

Chang. Y.-B., Lim, M.T., Pope, G.A. et al. 1994. CO_2 Flow Patterns Under Multiphase Flow: Heterogeneous Field-Scale Conditions. *SPE Res Eval & Eng* **9** (3): 208–216. http://dx.doi.org/10.2118/22654-PA.

Chang, Y.-B., Pope, G.A., and Sepehrnoori, K. 1990. A Higher-Order Finite-Difference Compositional Simulator. *J. Pet. Sci. & Eng.* **5** (1): 35–50.http://dx.doi.org/10.1016/0920-4105(90)90004-M.

Coutinho, J.A.P., Jørgensen, M., and Stenby, E.H. 1995. Predictions of Three-Phase Regions in CO_2-Oil Mixtures. *J. Pet. Sci. & Eng.* **12** (3): 201–208.

Creek, J.L. and Sheffield, J.M. 1993. Phase Behavior, Fluid Properties, and Displacement Characteristics of Permian Basin Reservoir Fluid/CO_2 Systems. *SPE Res Eval & Eng* **8** (1): 34–42. http://dx.doi.org/10.2118/20188-PA.

Davenport, A.J. and Rowlinson, J.S. 1963. The Solubility of Hydrocarbons in Liquid Methane. *Trans. of the Faraday Society* **59:** 78–84.

Davenport, A.J., Rowlinson, J.S., and Saville, G. 1966. Solutions of Three Hydrocarbons in Liquid Methane. *Trans. of the Faraday Society* **62:** 322–327.

Deiters, U.K. and Pegg, I.L. 1989. Systematic Investigation of the Phase Behavior in Binary Fluid Mixtures. I. Calculations Based on the Redlich-Kwong Equation of State. *J. Chemical Physics* **90** (11): 6632–6641.

Deiters, U. and Schneider, G.M. 1976. Fluid Mixtures at High Pressures. Computer Calculations of the Phase Equilibria and the Critical Phenomena in Fluid Binary Mixtures From the Redlich-Kwong Equation of State. *Berichte der Bunsengesellschaft fuer Physikalische Chemie* **80** (12): 1316–1321.

DeRuiter, R.A., Nash, L.J., and Singletary, M.S. 1994. Solubility and Displacement Behavior of a Viscous Crude with CO_2 and Hydrocarbon Gases. *SPE Res Eval & Eng* **9** (2): 101–106. http://dx.doi.org/10.2118/20523-PA.

Dindoruk, B. 1992. *Analytical Theory of Multiphase, Multicomponent Displacement in Porous Media*. PhD dissertation, Stanford University, Stanford, California (June 1992).

Enick, R., Holder, G.D., and Morsi, B.I. 1985. Critical and Three Phase Behavior in the Carbon Dioxide/Tridecane System. *Fluid Phase Equilibria* **22** (2): 209–224.

Galindo, A. and Blas, F.J. 2002. Theoretical Examination of the Global Fluid Phase Behavior and Critical Phenomena in Carbon Dioxide + *n*-Alkane Binary Mixtures. *J. Physical Chemistry B* **106** (17): 4343–4564.

Gardner, J.W., Orr Jr., F.M., and Patel, P.D. 1981. The Effect of Phase Behavior on CO_2-Flood Displacement Efficiency. *J. Pet Tech* **33** (11): 2067–2081. http://dx.doi.org/10.2118/8367-PA.

Gauter, K. 1999. *Fluid Multiphase Behavior in Ternary Systems of Near-Critical CO_2*. PhD dissertation, Technical University of Berlin, Berlin, Germany (January 1999).

Gauter, K., Heidemann, R.A., and Peters, C.J. 1999. Modeling of Fluid Multiphase Equilibria in Ternary Systems of Carbon Dioxide as the Near-Critical Solvent and Two Low-Volatile Solutes. *Fluid Phase Equilibria* **158–160:** 133–141.

Godbole, S.P., Thele, K.J., and Reinbold, E.W. 1995. EOS Modeling and Experimental Observations of Three-Hydrocarbon-Phase Equilibria. *SPE Res Eval & Eng* **10** (2): 101–108. http://dx.doi.org/10.2118/24936-PA.

Gregorowicz, J. and de Loos, Th.W. 1996. Modeling of the Three Phase LLV Region for Ternary Hydrocarbon Mixtures With the Soave-Redlich-Kwong Equation of State. *Fluid Phase Equilibria* **118** (1): 121–132.

Grigg, R.B. and Siagian, U.W.R. 1998. Understanding and Exploiting Four-Phase Flow in Low-Temperature CO_2 Floods. Paper SPE 39790 presented at the SPE Permian Basin Oil and Gas Recovery Conference, Midland, Texas, 23–26 March. http://dx.doi.org/10.2118/39790-MS.

Guler, B., Wang, P., Delshad, M. et al. 2001. Three- and Four- Phase Flow Compositional Simulations of CO_2/NGL EOR. Paper SPE 71485 presented at the Annual Technical Conference and Exhibition, 30 September–3 October, New Orleans, Louisiana. http://dx.doi.org./10.2118/71485-MS.

Helfferich, F.G. 1981. Theory of Multicomponent, Multiphase Displacement in Porous Media. *SPE J.* **21** (1): 51–62.

Henry, R.L. and Metcalfe, R.S. 1983. Multiple-Phase Generation During Carbon Dioxide Flooding. *SPE J.* **23** (4): 595–601. http://dx.doi.org/10.2118/8812-PA.

Holm, L.W. and Josendal, V.A. 1974. Mechanisms of Oil Displacement by Carbon Dioxide. *J Pet Tech* **26** (12): 1427–1438. http://dx.doi.org/10.2118/4736-PA.

Holm, L.W. and Josendal, V.A. 1980. Discussion of Determination and Prediction of CO_2 Minimum Miscibility Pressures. Paper associated with Yellig, W.F. and Metcalfe, R.S. 1980. *J Pet Tech* **32** (1): 160–168.

Huang, E.T.S. and Tracht, J.H. 1974. The Displacement of Residual Oil by Carbon Dioxide. Paper SPE 4735 presented at the SPE Improved Oil Recovery Symposium, Tulsa, Oklahoma, 22-24 April. http://dx.doi.org/10.2118/4735-MS.

Jessen, K., Michelsen, M.L., and Stenby, E.H. 1998. Global Approach for Calculation of Minimum Miscibility Pressure. *Fluid Phase Equilibria* **153:** 251–263.

Johns, R.T. 1992. *Analytical Theory of Multicomponent Gas Drives With Two-Phase Mass Transfer*. PhD dissertation, Stanford University, Stanford, California (May 1992).

Johns, R.T. and Orr Jr., F.M. 1996. Miscible Gas Displacement of Multicomponent Oils. *SPE J.* **1** (1): 39–50. http://dx.doi.org/10.2118/30798-PA.

Johns, R.T., Sah, P., and Sabramanian, S.K. 2000. Effect of Gas Enrichment Above the MME on Oil Recovery in Enriched-Gas Floods. *SPE J.* **5** (3): 331–338. http://dx.doi.org/10.2118/65704-PA.

Khan, S.A. 1992. *An Expert System to Aid in Compositional Simulation of Miscible Gas Flooding*. PhD dissertation, University of Texas at Austin, Austin, Texas.

Khan, S.A., Pope, G.A., and Sepehrnoori, K. 1992. Fluid Characterization of Three-Phase CO_2/Oil Mixtures. Paper SPE 24130 presented at the SPE/DOE Enhanced Oil Recovery Symposium, Tulsa, Oklahoma, 2224 April. http://dx.doi.org/10.2118/24130-MS.

Kohn, J.P., Kim, Y.J., and Pan, Y.C. 1966. Partial Miscibility Phenomena in Binary Hydrocarbon Systems Involving Ethane. *J. Chem. & Eng. Data* **11** (3): 333–335.

LaForce, T.C. 2005. *Mathematics of Partially Miscible Three-Phase Flow*. PhD dissertation, University of Texas at Austin, Austin, Texas (May 2005).

LaForce, T.C. 2012. Insight From Analytical Solutions for Improved Simulation of Miscible WAG Flooding in One Dimension. *Comp. Geosci.* **16:** 1007–1020.

LaForce, T.C., Jessen, K., and Orr Jr., F.M. 2008a. Four-Component Gas/Water/Oil Displacements in One Dimension: Part I. Structure of the Conservation Law. *Transport in Porous Media* **71:** 199–216.

LaForce, T.C., Jessen, K., and Orr Jr., F.M. 2008b. Four-Component Gas/Water/Oil Displacements in One Dimension: Part II. Example Solutions. *Transport in Porous Media* **72:** 83–96.

LaForce, T.C. and Johns, R.T. 2005. Composition Routes for Three-Phase Partially Miscible Flow in Ternary Systems. *SPE J.* **10** (2): 161–174. http://dx.doi.org/10.2118/89438-PA.

LaForce, T.C. and Orr Jr., F.M. 2008. Development of Gas/Oil Miscibility in Water and Gas Injection. Paper SPE 116119 presented at the SPE Annual Technical Conference and Exhibition, Denver, Colorado, 21–24 September. http://dx.doi.org/116119-MS.

LaForce, T.C. and Orr Jr., F.M. 2009. Four-Component Gas/Water/Oil Displacements in One Dimension: Part III. Development of Miscibility. *Transport in Porous Media* **79**: 225–247.

Larson, L.L., Silva, M.K., Taylor, M.A. et al. 1989. Temperature Dependence of $L_1/L_2/V$ Behavior in CO_2/Hydrocarbon Systems. *SPE Res Eval & Eng* **4** (1): 105–114. http://dx.doi.org/10.2118/15399-PA.

Lim, M.T., Khan, S.A., Sepehrnoori, K. et al. 1992. Simulation of Carbon Dioxide Flooding Using Horizontal Wells. Paper SPE 24929 presented at the SPE Annual Technical Conference and Exhibition, Washington, DC, 4–7 October. http://dx.doi.org/10.2118/24929-MS.

Lohrenz, J., Bray, B.C., and Clark, C.R. 1964. Calculating Viscosities of Reservoir Fluids From Their Compositions. *J. Pet Tech* **16** (10): 1171–1176.

McKean, T.A.M., Thomas, A.H., Chesher, J.R. et al. 1999. Schrader Bluff CO_2 EOR Evaluation. Paper SPE 54619 presented at the SPE Western Regional Meeting, Anchorage, Alaska, 26–27 May. http://dx.doi.org/10.2118/54619-MS.

Metcalfe, R.S. and Yarborough, L. 1979. The Effect of Phase Equilibria on the CO_2 Displacement Mechanism. *SPE J.* **19** (4): 242–252. http://dx.doi.org/10.2118/7061-PA.

Mohanty, K.K., Masino Jr., W.H., Ma, T.D. et al. 1995. Role of Three-Hydrocarbon-Phase Flow in a Gas-Displacement Process. *SPE Res Eval & Eng* **10** (3): 214–221. http://dx.doi.org/10.2118/24115-PA.

Mushrif, S.H. 2004. *Determining Equation of State Binary Interaction Parameters Using* K- *and* L-*Points*. MS thesis, University of Saskatchewan, Saskatoon, Canada (October 2004).

Mushrif, S.H. and Phoenix, A.V. 2008. Effect of Peng-Robinson Binary Interaction Parameters on the Predicted Multiphase Behavior of Selected Binary Systems. *Industrial and Eng. Chemistry Res.* **47** (16): 6280–6288.

Negahban, S. and Kremesec Jr., V.J. 1992. Development and Validation of Equation-of-State Fluid Descriptions for CO_2/Reservoir-Oil Systems. *SPE Res Eval & Eng* **7** (3): 363–368.

Ogino, K. 1988. *Compositional Simulation of Carbon Dioxide Oil Recovery Experiments*, MS thesis, University of Texas at Austin, Austin, Texas.

Okuno, R. 2009. *Modeling of Multiphase Behavior for Gas Flooding Simulation*. PhD dissertation, the University of Texas at Austin, Austin, Texas (August 2009).

Okuno, R., Johns, R.T., and Sepehrnoori, K. 2011. Mechanisms for High Displacement Efficiency of Low-Temperature CO_2 Floods. *SPE J.* **16** (4): 751–767. http://dx.doi.org/10.2118/129846-PA.

Okuno, R. and Xu, Z. 2014. Efficient Displacement of Heavy Oil by Use of Three Hydrocarbon Phases. *SPE J.* SPE-165470-PA. (in press; published online 12 March 2014). http://dx.doi.org/10.2118/165470-PA.

Okuyiga, M.O. 1992. Equation of State Characterization and Miscibility Development in a Multiple Phase Hydrocarbon System. Paper SPE 24937 presented at the Annual Technical Conference and Exhibition, Washington, DC, 4–7 October. http://dx.doi.org/10.2118/24937-MS.

Orr Jr., F.M. 2007. *Theory of Gas Injection Processes*. Holte, Denmark: Tie-Line Publications.

Orr Jr., F.M. and Jensen, C.M. 1984. Interpretation of Pressure-Composition Phase Diagrams for CO_2/Crude-Oil Systems. *SPE J.* **24** (5): 485–497. http://dx.doi.org/10.2118/11125-PA.

Orr Jr., F.M., Silva, M.K., and Lien, C.L. 1983. Equilibrium Phase Compositions of CO_2/Crude Oil Mixtures—Part 2: Comparison of Continuous Multiple-Contact and Slim-Tube Displacement Tests. *SPE J.* **23** (2): 281–291. http://dx.doi.org/10.2118/10725-PA.

Orr Jr., F.M., Yu, A.D., and Lien, C.L. 1981. Phase Behavior of CO_2 and Crude Oil in Low-Temperature Reservoirs. *SPE J.* **21** (4): 480–492. http://dx.doi.org/10.2118/8813-PA.

PVTsim, 20.0. 2011. Calsep A/S, Lyngby, Denmark.

Rowlinson, J.S. and Freeman, P.I. 1961. Lower Critical Solution Points in Hydrocarbon Mixtures. *Pure and Applied Chemistry* **2** (1–2): 329–334.

Scott, R.L. and van Konynenburg, P.H. 1970. van der Waals and Related Models for Hydrocarbon Mixtures. *Discussions of the Faraday Society* **49:** 87–97.

Shelton, J.L. and Yarborough, L. 1977. Multiple Phase Behavior in Porous Media During CO_2 or Rich-Gas Flooding. *J. Pet Tech* **29** (9):1171–1178. http://dx.doi.org/10.2118/5827-PA.

Stalkup, F.I. 1978. Carbon Dioxide Miscible Flooding: Past, Present, and Outlook for the Future. *J. Pet Tech* **30** (8): 1102–1112. http://dx.doi.org/10.2118/7042-PA.

Tchelepi, H.A. and Orr Jr., F.M. 1994. Interaction of Viscous Fingering, Permeability Heterogeneity, and Gravity Segregation in Three Dimensions. *SPE Res Eval & Eng* **9** (4): 266–271. http://dx.doi.org/10.2118/25235-PA.

Turek, E.A., Metcalfe, R.S., and Fishback, R.E. 1988. Phase Behavior of Several CO_2/West Texas-Reservoir-Oil Systems. *SPE Res Eval & Eng* **3** (2): 505–516. http://dx.doi.org/10.2118/13117-PA.

Uzunov, D.I. 1993. *Introduction to the Theory of Critical Phenomena*. Farrer Road, Singapore: World Scientific Publishing.

van Konynenburg, P.H. 1968. *Critical Lines and Phase Equilibria in Binary Mixtures*. PhD dissertation, University of California, Los Angeles, California.

van Konynenburg, P.H. and Scott, R.L. 1980. Critical Lines and Phase Equilibria in Binary van der Waals Mixtures. *Philosophical Trans. of the Royal Society of London. Series A, Math. & Physical Sci.* **298** (1442): 495–540.

Wagner, J.R., McCaffrey, D.S., and Kohn, J.P. 1968. Partial Miscibility Phenomena in the Ternary System Ethane-*n*-Hexadecane-*n*-Eicosane. *J. Chem. & Eng. Data* **13** (1): 22–24.

Wang, Y., Lin, C.-Y., Bidinger, C. et al. 2003. Compositional Modeling of Gas Injection With Three Hydrocarbon Phases for Schrader Bluff EOR. Paper SPE 84180 presented at the SPE Annual Technical Conference and Exhibition, Denver, Colorado, 5–8 October. http://dx.doi.org/10.2118/84180-MS.

Wang, Y. and Orr Jr., F.M. 1997. Analytical Calculation of Minimum Miscibility Pressure. *Fluid Phase Equilibria* **139:** 101–124.

Yang, Q. 2006. *Automatic Development of Global Phase Diagrams for Binary Systems in Pressure-Temperature Space*. Master thesis, University of Saskatchewan, Saskatoon, Canada (August 2006).

Yellig, W.F. and Metcalfe, R.S. 1980. Determination and Prediction of CO_2 Minimum Miscibility Pressures. *J. Pet Tech* **32** (1): 160–168. http://dx.doi.org/10.2118/7477-PA.

Appendix A—Schematic of a Three-Phase Region Bounded by CEP Tie Lines

A three-phase region has one degree of freedom at a given temperature and pressure for four components. Therefore, a three-phase region is a volumetric region in a quaternary diagram. The three-

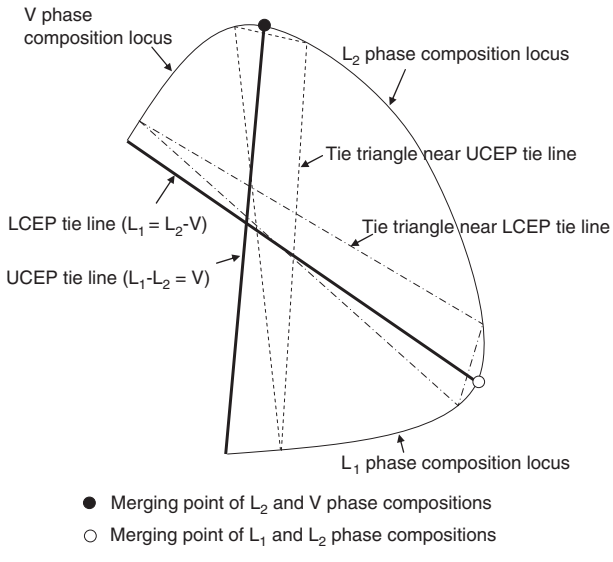

Fig. A-1—Schematic of a three-phase region bounded by critical endpoint (CEP) tie lines for a quaternary system at a fixed temperature and pressure.

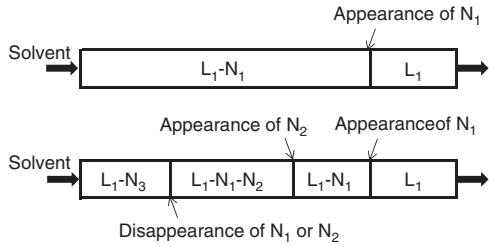

Fig. B-1—Schematics of phase behavior in two- and three-phase displacements. The oleic phase is given as L_1. A nonoleic phase (N_1) appears at the displacement front for two- and three-phase displacements. For a three-phase displacement, another nonoleic phase (N_2) appears at the leading edge of the three-phase region. One of the two nonoleic phases (N_1 and N_2) in the three-phase region disappears at the trailing edge of the three-phase region. The nonoleic phase (N_3) in the upstream two-phase region is either N_1 or N_2 depending on the phase behavior involved there.

phase region consists of an infinite number of tie triangles. A tie triangle changes its shape and size within the three-phase region. Two tie triangles are shown to illustrate tie triangles exhibiting near-CEP behavior. A CEP is not a point in composition space, but is a tie line in which two of the three phases are critical in the presence of the other noncritical phase. The UCEP typically occurs at higher solvent concentrations than the LCEP, as observed for CO_2-*n*-alkane and *n*-alkane binaries. More details on three-hydrocarbon-phase behavior predictions are given in Okuno (2009).

Appendix B—Schematics of Phase Behavior in Two- and Three-Phase Displacements

A two-phase displacement involves the L_1 phase and a non-oleic (N_1) phase. Although the N_1 phase is often the V phase because of a fast traveling methane bank, we do not specify its phase identity in the schematic for generality. A phase transition between one and two phases occurs at the displacement front, in which the N_1 phase appears. Complete evaporation of the L_1 phase is invisible in the schematic because the evaporation wave is normally much slower than the displacement front, especially in the presence of dispersion.

Phase behavior for three-phase displacement of oil is more involved. Two nonoleic phases appear in sequence in the direction from the producer to the injector. The nonoleic phase that appears first at the displacement front is referred to as N_1. The N_2 phase then appears at the leading edge of the three-phase region, which is at equilibrium with the L_1 and N_1 phases in the three-phase region. One of the two nonoleic phases disappears at the trailing edge of the three-phase region. The nonoleic phase that coexists with the L_1 phase in the upstream two-phase region is referred to as N_3, which is either N_1 or N_2, depending on the phase transition there.

There are four patterns for phase transitions for the three-phase displacement in Fig. B-1 because the N_1-N_3 pair can be either V-V, or V-L_2, or L_2-V, or L_2-L_2 [i.e., the four patterns for (N_1, N_2, N_3) are as follows: (V, L_2, V), (V, L_2, L_2), (L_2, V, V), and (L_2, V, L_2)]. The two phases at the displacement front are typically the V and L_1 phases because of a fast-travelling methane bank. For the two phases upstream of the three-phase region, however, both L_1-V and L_1-L_2 are common, depending on phase behavior near the injection gas composition at the operating temperature and pressure. Although it is possible to have a direct transition between one phase and three phases without involving two-phase equilibrium, this type of phase transition is not considered in this research.

Appendix C—Mass Conservation on Multiphase Transitions in Finite-Difference Simulation

Conservation of mass for a component in N_P-phase flow through porous media is considered with the following assumptions:

- 1D flow with no gravity
- constant temperature
- change in pressure is small across the displacement length
- constant porosity with time
- no diffusion/dispersion
- no chemical reaction or sorption on the solid phase
- no capillary pressure
- local equilibrium
- ideal mixing
- laminar flow.

We then obtain

$$\frac{\partial C_i}{\partial t_D}+\frac{\partial F_i}{\partial x_D}=0, \quad \ldots\ldots\ldots\ldots\ldots\ldots\ldots\ldots \text{(C-1)}$$

where t_D is the dimensionless time measured in pore volumes, x_D is the dimensionless distance from the injector, C_i is the overall volume fraction of component i, F_i is the overall fractional flow of component i, and $i=1, 2,\ldots, (N_C-1)$. C_i and F_i are given as

$$C_i=\sum_{j=1}^{N_P} S_j c_{ij} \text{ and}$$

$$F_i=\sum_{j=1}^{N_P} f_j c_{ij},$$

where S_j is the saturation of phase j, f_j is the fractional flow of phase j, and c_{ij} is the volume fraction of component i in phase j. A detailed derivation of Eq. C-1 is given in Orr (2007).

The weak form of Eq. C-1 is

$$\frac{d}{dt_D}\int C_i dV+\int n\cdot F_i dS=0, \quad \ldots\ldots\ldots\ldots\ldots\ldots \text{(C-2)}$$

where V and S are the volume and surface area of the control volume of interest, respectively; n is the outward normal unit vector on surface S. Let us consider two consecutive gridblocks in a 1D simulation model, where N_P^U and N_P^D phases are present in the upstream and downstream cells, respectively, at a given time. A uniform grid size of Δx_D is considered.

Suppose a phase transition between N_P^U and N_P^D propagates at a dimensionless velocity of $v_D=\Delta x_D/\Delta t_D$, where Δt_D is a certain time period in pore volumes. Discretization of Eq. C-2 with Δx_D and Δt_D by use of the one-point upstream weighting for the flux term yields

$$v_D=\frac{\Delta x_D}{\Delta t_D}=\frac{F_i^U-F_i^D}{C_i^U-C_i^D}. \quad \ldots\ldots\ldots\ldots\ldots\ldots\ldots \text{(C-3)}$$

Rearrangement of Eq. C-3 gives

$$\sum_{j=1}^{N_P^U}(v_D S_j^U-f_j^U)\underline{c}_j^U=\sum_{j=1}^{N_P^D}(v_D S_j^D-f_j^D)\underline{c}_j^D, \quad \ldots\ldots \text{(C-4)}$$

where $\underline{c}_j$ is a vector consisting of c_{ij}. Dividing Eq. C-4 by (v_D-1),

$$\sum_{j=1}^{N_P^U}\gamma_j^U\underline{c}_j^U=\sum_{j=1}^{N_P^D}\gamma_j^D\underline{c}_j^D, \quad \ldots\ldots\ldots\ldots\ldots\ldots \text{(C-5)}$$

where $\gamma_j^U=\dfrac{v_D S_j^U-f_j^U}{v_D-1}$ and $\gamma_j^D=\dfrac{v_D S_j^D-f_j^D}{v_D-1}$. Note that $\sum_{j=1}^{N_P^U}\gamma_j^U=1.0$, and $\sum_{j=1}^{N_P^D}\gamma_j^D=1.0$.

Eq. C-5 is of the identical form with the generalized jump conditions on multiphase transition presented in Okuno and Xu (2014). The difference is that v_D in Eq. C-5 is, in general, not the same as the shock velocity of the corresponding multiphase transition in the MOC solution. In other words, $\underline{c}_j^U$ and $\underline{c}_j^D$ are affected by numerical dispersion caused by the discretization. Eq. C-5 explains that components are redistributed on a multiphase transition through an intersection of the tie simplex extension of (N_P^D-1) dimensions with that of (N_P^U-1) dimensions. Eq. C-5 can be used for mechanistic interpretation of mass transfer on a multiphase transition even in the presence of numerical dispersion.

Eq. C-5 in composition space is

$$\underline{z}^{\text{int}} = \sum_{j=1}^{N_P^U} \Gamma_j^U \, \underline{x}_j^U = \sum_{j=1}^{N_P^D} \Gamma_j^D \, \underline{x}_j^D, \quad \ldots\ldots\ldots\ldots \text{(C-6)}$$

where $\sum_{j=1}^{N_P^U} \Gamma_j^U = \sum_{j=1}^{N_P^D} \Gamma_j^D = 1.0$. The intersection composition is $\underline{z}^{\text{int}}$. The Γ parameters give the relative location of $\underline{z}^{\text{int}}$ with respect to the corresponding tie simplex. For example, the Γ_j^U parameters give the location of $\underline{z}^{\text{int}}$ relative to the tie simplex defined by N_P^U phase compositions $\underline{x}_j$, where $j = 1, 2, \ldots, N_P^U$.

SI Metric Conversion Factors

ft × 3.048*	E−01 = m
°F (°F − 32)/1.8	= °C
psi × 6.894 757	E+00 = kPa

*Conversion factor is exact.

Ryosuke Okuno has served as assistant professor of petroleum engineering in the Department of Civil and Environmental Engineering at the University of Alberta since 2010. His research and teaching interests include enhanced oil recovery (EOR), thermal oil recovery, oil-displacement theory, numerical reservoir simulation, thermodynamics, multiphase behavior, and applied mathematics. Okuno has seven years of industrial experience as a reservoir engineer with Japan Petroleum Exploration Co., Ltd., and is a registered professional engineer in Alberta, Canada. He holds BE and ME degrees in geosystem engineering from the University of Tokyo, and a PhD degree in petroleum engineering from the University of Texas at Austin. Okuno is an SPE member.

Zhongguo Xu is a PhD candidate in petroleum engineering in the Department of Civil and Environmental Engineering at the University of Alberta. His research interests include numerical reservoir simulation and multiphase behavior. Xu holds a BS degree from the China University of Petroleum (Beijing) and an MEng degree from the University of Alberta, both in petroleum engineering. Xu is an SPE member.